

Understanding the Masses and Mixings of One-Zero Textures in 3+1 Scenario

Newton Nath,^{1,2,*} Monojit Ghosh,^{1,†} and Shivani Gupta^{3,‡}

¹*Physical Research Laboratory, Navrangpura, Ahmedabad 380 009, India*

²*Indian Institute of Technology, Gandhinagar, Ahmedabad-382424, India*

³*Center of Excellence in Particle Physics (CoEPP), University of Adelaide, Adelaide SA 5005, Australia*

We present a detailed analysis and phenomenological consequences of neutrino mass matrix, M_ν , with one-zero texture in the flavor basis where the active neutrino sector is extended by one sterile neutrino (3+1 case). In particular, our aim is to explore behaviour of the sterile mixing parameters in detail when one of the elements of the neutrino mass matrix goes to zero. To study this, we consider two distinct mass spectrum of the active neutrinos: (i) completely hierarchical mass spectrum with a vanishing neutrino mass and (ii) completely quasidegenerate mass spectrum. In 3+1 scenario, the low energy neutrino mass matrix, M_ν , is a 4×4 matrix and has 10 independent elements. Thus it can have 10 possible one-zero textures. From the earlier studies it can be inferred that, if one assumes one vanishing neutrino mass, then only seven of these M_ν are phenomenologically allowed by the current neutrino oscillation data. On the other hand, if the neutrinos are quasidegenerate then there are eight phenomenologically viable one-zero textures. In this present work, we study the correlations between the sterile mixing parameters for each of these allowed textures for both mass spectrum and also their implications on the effective Majorana mass.

I. INTRODUCTION

Compelling evidence have been provided by solar, atmospheric, reactor and accelerator neutrinos for the existence of neutrino oscillations among the three active neutrinos. Neutrino oscillation in three generation can be described by three mixing angles: θ_{12} , θ_{23} and θ_{13} , two mass squared differences: $\Delta m_{21}^2 (m_2^2 - m_1^2)$ and $\Delta m_{31}^2 (m_3^2 - m_1^2)$ and one Dirac type CP phase δ_{CP} . There are two additional phases if neutrinos are Majorana particles. The global fits of neutrino oscillation data in the framework of 3ν mixing [1–3] give us precise values of the neutrino oscillation parameters. At present, the major unknowns in the three flavour oscillation picture are: (i) the sign of the atmospheric mass squared difference Δm_{31}^2 i.e., whether the neutrino mass hierarchy is normal or inverted ($\Delta m_{31}^2 > 0$: NH or $\Delta m_{31}^2 < 0$: IH), (ii) the octant of θ_{23} i.e., lower or higher ($\theta_{23} < 45^\circ$: LO or $\theta_{23} > 45^\circ$: HO) and (iii) the precise value of the leptonic CP phase δ_{CP} . There are various current ongoing / future upcoming neutrino oscillation experiments dedicated to the determination of the remaining unknown oscillation parameters.

Another intriguing aspect of current neutrino physics is the existence of light sterile neutrino. Sterile neutrinos are $SU(2)$ singlet which implies that they do not take part in the usual weak interactions. However, they can mix with the active neutrinos and thus probed in the neutrino oscillation experiments. The oscillation results of the LSND experiment shows the evidence that there should be at least one sterile neutrino having mass in the \sim eV scale [4–6]. The latest antineutrino data of MiniBooNE also have some overlap with the the allowed regions of the LSND experiment supporting the sterile neutrino hypothesis [7].¹ In addition, studies of reactor antineutrino spectra show a 3% enhancement in the fluxes as compared to

the previous calculation. With these new re-evaluated fluxes, the ratio of observed event rate to predicted rate for < 100 m reactor experiments shifts from 0.976 to 0.943, giving rise to reactor neutrino anomaly [8]. This deficit can not be explained in three flavour framework and evokes the presence of sterile neutrinos. The recently observed Gallium anomaly also seems to support the sterile neutrino hypothesis [9]. Although it is possible to fit experimental data with more than one light sterile neutrinos, the 3+1 hypothesis i.e., three active neutrinos in the sub-eV scale and one eV scale sterile neutrino, is considered to be minimal and still not completely ruled out from the cosmological observations. Recent analysis of the Planck data shows that the possibility of light sterile neutrino is ruled at 3σ within the Λ CDM model. However it is possible to have one light sterile neutrino in the eV scale if one deviates slightly from the base Λ CDM model [10]. The possibility of having more than one light sterile neutrino is highly disfavoured in cosmology. In the 3+1 model, there are total six mixing angles, three Dirac phases, three Majorana phases and three mass squared differences. The new mixing angles, which arise due to the inclusion of one sterile neutrino, are θ_{14} , θ_{24} and θ_{34} . The additional mass squared difference is Δm_{LSD}^2 which can be either Δm_{41}^2 if the active neutrinos are normal hierarchical or Δm_{43}^2 when the active neutrinos are inverted hierarchical.

Neutrino mass matrices provide important tool for the investigation of underlying symmetries and resulting dynamics. The first step in this direction is to construct the neutrino mass matrix in the flavor basis. However, the reconstruction results in a large variety of possible structures of the mass matrices depending strongly on the mass scale, mass hierarchy and the Majorana phases. Several proposals have been made in literature to restrict the form of neutrino mass matrix and to reduce the number of free parameters one of which is the zero texture. Zero texture implies that one or more elements are

* Email Address: newton@prl.res.in

† Email Address: monojit@prl.res.in

‡ Email Address: shivani.gupta@adelaide.edu.au

¹ Note that the excess of the MiniBooNE neutrino data marginally agrees

with a simple two neutrino oscillation formalism and requires more data to resolve the issue.

relatively small compared to others. Extensive studies of neutrino mass matrices with zero textures in the standard three neutrino scenario have been done in [11–22]. These neutrino mass matrix textures, in general, may be obtained by imposing certain Abelian family symmetries [23–25]. For the three generations the maximum number of zero textures in neutrino mass matrix is two whereas the addition of a sterile neutrino to the standard three neutrino picture (3+1) can increase the allowed zero textures to three [26–28].

In this paper we investigate the phenomenology of the one-zero textures in the low energy neutrino mass matrix for 3+1 scheme. In particular, our main focus in this present work is to understand the mixing pattern of the sterile parameters which give rise to allowed one-zero textures. The study of one-zero texture in 3+1 scheme has been done in [27]. The paper mainly studied the nature of the matrix elements as a function of the lowest mass. This facilitates to identify the mass ranges over which it is possible to have one-zero texture for a given matrix element. However, in this paper the main emphasis is to study the correlations between the different active sterile mixing parameters. To understand this, the strategy of the present work is as follows. We consider two distinct mass spectrum: (i) the completely hierarchical mass spectrum in which the lowest active neutrinos mass is zero² and (ii) the quasidegenerate mass spectrum where all the three active neutrinos have mass of the same order. From the results of [27], one can infer that for completely hierarchical mass spectrum the number of allowed texture is seven and if one considers quasidegenerate spectrum then eight one-zero textures become allowed. In this paper we study the correlation between different sterile mixing parameters for every allowed one-zero textures corresponding to the above two mass spectrum. These results are important to understand the underlying parameter space of the neutrino mass matrix and they can also help in putting constraint on the free parameters of the models involving light sterile neutrinos [30–32].

The plan of the paper goes as follows. In Section II, we present the mass and mixing patterns along with the experimental constraints on the neutrino oscillation parameters when a sterile neutrino of mass ~ 1 eV is added to standard three neutrino picture. In Section III we present our formalism for obtaining one-zero textures assuming: (a) the lowest neutrino mass to vanish and (b) the masses of active neutrinos are quasidegenerate i.e., approximately of same order. In Section IV we study the phenomenological consequences of all the ten elements of the mass matrix for the above mentioned scenarios. We also present the predictions on effective Majorana mass, governing neutrinoless double beta decay for all the phenomenologically viable textures. We finally conclude in Section V.

II. MASSES AND MIXINGS IN 3+1 SCENARIO AND EXPERIMENTAL CONSTRAINTS

The sterile state of mass \sim eV can be added to the standard three neutrino mass states in two different ways. In one case active neutrinos have normal hierarchical mass spectrum i.e.,

SNH: $m_1 \approx m_2 < m_3 < m_4$ which implies,

$$m_2 = \sqrt{m_1^2 + \Delta m_{21}^2}, \quad (1)$$

$$m_3 = \sqrt{m_1^2 + \Delta m_{21}^2 + \Delta m_{31}^2}, \quad (2)$$

$$m_4 = \sqrt{m_1^2 + \Delta m_{41}^2}. \quad (3)$$

Here m_1, m_2 and m_3 are active neutrino masses and m_4 is the sterile neutrino mass.

In the second case the active neutrinos will be inverted hierarchical i.e.,

SIH: $m_3 < m_1 \approx m_2 < m_4$ implying

$$m_1 = \sqrt{m_3^2 + \Delta m_{31}^2}, \quad (4)$$

$$m_2 = \sqrt{m_3^2 + \Delta m_{31}^2 + \Delta m_{21}^2}, \quad (5)$$

$$m_4 = \sqrt{m_3^2 + \Delta m_{43}^2}. \quad (6)$$

The mass spectrum for SNH and SIH are displayed in Fig. 1.

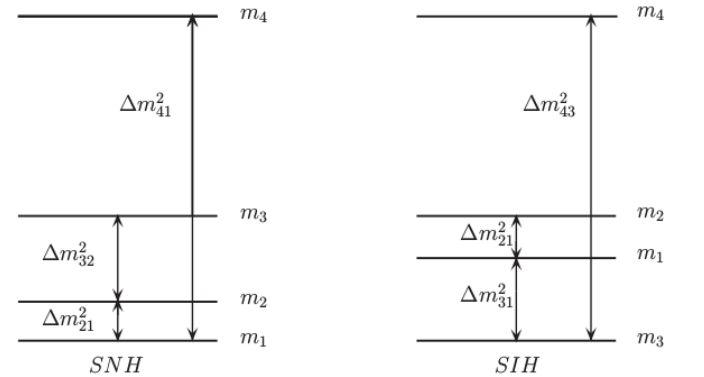


FIG. 1. Allowed mass spectrum in 3+1 scheme for normal (SNH) and inverted (SIH) hierarchy.

In the 3+1 scenario, the 4×4 Majorana neutrino mass matrix, M_ν , in the flavor basis can be diagonalized as

$$M_\nu = V M_\nu^{diag} V^T, \quad (7)$$

where $M_\nu^{diag} = \text{diag}\{m_1, m_2, m_3, m_4\}$ is the diagonal neutrino mass matrix. The matrix V is the leptonic mixing matrix in the basis where the charged lepton mass matrix is diagonal [35] and is given as

$$V = U.P. \quad (8)$$

In general, any arbitrary $N \times N$ unitary matrix contains $\frac{N(N-1)}{2}$ mixing angles and $\frac{1}{2}(N-1)(N-2)$ Dirac type CP

² The one-zero singular models are found to be quite rich in phenomenology in comparison to non singular models for 3 active neutrinos [29].

Parameter	Best Fit $\pm 1\sigma$	2σ range	3σ range
$\Delta m_{21}^2 [10^{-5} \text{ eV}^2]$	$7.60^{+0.19}_{-0.18}$	$7.26 - 7.99$	$7.11 - 8.18$
$\Delta m_{31}^2 [10^{-3} \text{ eV}^2] \text{ (NH)}$	$2.48^{+0.05}_{-0.07}$	$2.35 - 2.59$	$2.30 - 2.65$
$\Delta m_{31}^2 [10^{-3} \text{ eV}^2] \text{ (IH)}$	$2.38^{+0.05}_{-0.06}$	$2.26 - 2.48$	$2.20 - 2.54$
$\sin^2 \theta_{12}/10^{-1}$	3.23 ± 0.16	$2.92 - 3.57$	$2.78 - 3.75$
$\sin^2 \theta_{13}/10^{-2} \text{ (NH)}$	2.26 ± 0.12	$1.95 - 2.74$	$1.90 - 2.62$
$\sin^2 \theta_{13}/10^{-2} \text{ (IH)}$	2.29 ± 0.12	$2.02 - 2.78$	$1.93 - 2.65$
$\sin^2 \theta_{23}/10^{-1} \text{ (NH)}$	$5.67^{+0.32}_{-1.24}$	$4.13 - 6.23$	$3.93 - 6.43$
$\sin^2 \theta_{23}/10^{-1} \text{ (IH)}$	$5.73^{+0.25}_{-0.39}$	$4.32 - 6.21$	$4.03 - 6.40$
$\Delta m_{\text{LSND}}^2 (\text{eV}^2)$	$0.89^{+0.16}_{-0.11}$	$0.73 - 2.05$	$0.7 - 2.5$
$\sin^2 \theta_{14}$	$0.025^{+0.025}_{-0.015}$	$0.013 - 0.05$	$0.01 - 0.06$
$\sin^2 \theta_{24}$	$0.023^{+0.004}_{-0.008}$	$0.005 - 0.035$	$0.003 - 0.04$
$\sin^2 \theta_{34}$	—	—	< 0.18

TABLE I. Best-fit and 3σ ranges of active neutrino oscillation parameters as given in [1–3]. The current constraints on sterile neutrino parameters are from the global analysis as given in [33, 34]. Here, $\Delta m_{\text{LSND}}^2 (\text{eV}^2)$ is either $\Delta m_{41}^2 (\text{eV}^2)$ or $\Delta m_{43}^2 (\text{eV}^2)$.

phases. If the neutrinos are Majorana particles there will be additional $(N - 1)$ Majorana phases. Here U is the lepton mixing matrix for Dirac neutrinos and can be written as

$$U = R_{34} \tilde{R}_{24} \tilde{R}_{14} R_{23} \tilde{R}_{13} R_{12}, \quad (9)$$

where R_{ij} denotes rotation matrices in the ij generation space and is expressed as,

$$R_{23} = \begin{pmatrix} 1 & 0 & 0 & 0 \\ 0 & c_{23} & s_{23} & 0 \\ 0 & -s_{23} & c_{23} & 0 \\ 0 & 0 & 0 & 1 \end{pmatrix},$$

$$\tilde{R}_{13} = \begin{pmatrix} c_{13} & 0 & s_{13}e^{-i\delta_{13}} & 0 \\ 0 & 1 & 0 & 0 \\ -s_{13}e^{i\delta_{13}} & 0 & c_{13} & 0 \\ 0 & 0 & 0 & 1 \end{pmatrix},$$

where $s_{ij} = \sin \theta_{ij}$ and $c_{ij} = \cos \theta_{ij}$. The mixing matrix U is parameterized in terms of six mixing angles: θ_{12} , θ_{23} , θ_{13} , θ_{14} , θ_{24} and θ_{34} and three Dirac CP violating phases: δ_{13} , δ_{14} , δ_{24} . The diagonal phase matrix P in Eq (8) is given as,

$$P = \text{diag}\{1, e^{i\alpha}, e^{i(\beta+\delta_{13})}, e^{i(\gamma+\delta_{14})}\}, \quad (10)$$

where α , β and γ are three Majorana CP violating phases. Table. I, gives the current best-fits and 3σ ranges of the mixing parameters. Oscillation parameters for active neutrinos are taken from [1–3] and sterile mixing parameters are taken from [34, 36].

Oscillation experiments can measure only the mass squared differences and give no information on the absolute neutrino masses. Information on absolute masses can come from neutrinoless double beta decay ($0\nu\beta\beta$) experiments. Double beta

decay experiments will observe the lepton number violating process and probe the Majorana nature of neutrinos. Neutrinoless double beta decay processes are sensitive to effective Majorana mass which in 3+1 scenario is given as

$$\begin{aligned} M_{ee} &= |\Sigma U_{ei}^2 m_i| \\ &= |(U_{e1})^2 m_1 + (U_{e2})^2 m_2 e^{2i\alpha} \\ &\quad + (U_{e3})^2 m_3 e^{2i(\beta+\delta_{13})} + (U_{e4})^2 m_4 e^{2i(\gamma+\delta_{14})}| \\ &= |m_1 c_{12}^2 c_{13}^2 c_{14}^2 + m_2 e^{2i\alpha} c_{13}^2 c_{14}^2 s_{12}^2 \\ &\quad + m_3 e^{2i\beta} s_{13}^2 c_{14}^2 + m_4 e^{2i\gamma} s_{14}^2|. \end{aligned} \quad (11)$$

We see that M_{ee} is sensitive to the Majorana phases which are present in the neutrino mass matrix. A large number of projects such as CUORE [37], GERDA [38], SuperNEMO [39], KamLAND-ZEN [40] and EXO [41] aim to discover evidences for neutrinoless double beta decay. These experiments also put bounds on the effective Majorana mass M_{ee} . These experiments are expected to achieve a sensitivity upto 0.01 eV for M_{ee} . The combined results from KamLAND-ZEN and EXO-200 [40] give the upper bound on the effective Majorana neutrino mass as $M_{ee} < (0.12 - 0.25) \text{ eV}$, where the range comes from uncertainty in the nuclear matrix elements. The next generation experiments are expected to improve the bounds and the sensitivity to $M_{ee} < (0.0080 \pm 0.0016) \text{ eV}$ [42].

III. FORMALISM

One-zero texture neutrino mass matrix results in the following condition

$$\begin{aligned} m_1 U_{a1} U_{b1} + m_2 U_{a2} U_{b2} e^{2i\alpha} \\ + m_3 U_{a3} U_{b3} e^{2i(\beta+\delta_{13})} + m_4 U_{a4} U_{b4} e^{2i(\gamma+\delta_{14})} = 0 \end{aligned} \quad (12)$$

where a, b can be e, μ, τ and s . We study the zero texture in 4×4 neutrino mass matrix taking: (i) vanishing lowest mass i.e., $m_1 = 0$ for NH (A) and $m_3 = 0$ for IH (B) and (ii) the three active masses are almost equal i.e., $m_1 \sim m_2 \sim m_3$ (C).

A. Normal Hierarchy

For normal hierarchy, one textures with a vanishing lowest mass ($m_1 = 0$), Eq. (12) can be written as,

$$p U_{a2} U_{b2} + U_{a3} U_{b3} e^{2i(\beta+\delta_{13})} + q U_{a4} U_{b4} e^{2i(\gamma+\delta_{14})} = 0. \quad (13)$$

Here, $p = \frac{m_2}{m_3} e^{2i\alpha}$ and $q = \frac{m_4}{m_3}$.

Solving the above equation constrains p as

$$p = - \left(\frac{U_{a3} U_{b3} e^{2i(\beta+\delta_{13})} + q U_{a4} U_{b4} e^{2i(\gamma+\delta_{14})}}{U_{a2} U_{b2}} \right). \quad (14)$$

The neutrino mass ratio for normal hierarchy is

$$\frac{m_2}{m_3} = |p|$$

and one of the physical Majorana phase α is given as

$$\alpha = \frac{1}{2} \arg(p). \quad (15)$$

The total number of free parameters is five, three Dirac and two Majorana CP phases. Note that we have assumed one of the active neutrino mass to vanish so the number of physical phases is two. For example we can always take the phase β out of the Eq. (13) and the physical Majorana phases will be $(\alpha - \beta)$ and $(\gamma - \beta)$. The condition of vanishing lowest mass ensures that all the remaining three masses are well determined from the experimental mass squared difference. The remaining three masses for normal hierarchy are found in terms of mass squared differences as $m_2 = \sqrt{\Delta m_{21}^2}$, $m_3 = \sqrt{\Delta m_{21}^2 + \Delta m_{31}^2}$ and $m_4 = \sqrt{\Delta m_{41}^2}$. We span the parameter space of input neutrino oscillation parameters (3 active and 3 active sterile mixing angles) lying in their 3σ ranges by randomly generating points to the order of 10^9 . Since the Dirac CP phases are experimentally unconstrained at 3σ level,

therefore, we vary them within their full possible range $[0^\circ - 360^\circ]$. We can find two independent mass squared difference ratios defined as,

$$\begin{aligned} R_\nu &= \frac{\Delta m_{21}^2}{\Delta m_{32}^2} = \frac{|p|^2}{1 - |p|^2}, \\ R_{\nu_1} &= \frac{\Delta m_{41}^2}{\Delta m_{32}^2} = \frac{q^2}{1 - |p|^2}. \end{aligned} \quad (16)$$

The allowed 3σ ranges for these mass squared difference ratios is

$$\begin{aligned} R_\nu &= (2.7 \times 10^{-2} - 3.5 \times 10^{-2}), \\ R_{\nu_1} &= (0.26 \times 10^3 - 1.08 \times 10^3). \end{aligned} \quad (17)$$

The given texture is viable if the mass squared difference ratios are in their current 3σ ranges. Since we consider the neutrino mass matrices with lowest vanishing mass ($m_1 = 0$ for NH), in that case using the fact that $R_\nu \ll 1$, the masses in terms of R_ν and R_{ν_1} can be rewritten as,

$$\text{SNH} : |m_4| \approx \sqrt{\Delta m_{31}^2 R_{\nu_1}} \gg |m_3| \approx \sqrt{(1 + R_\nu) \Delta m_{31}^2} \approx \sqrt{\Delta m_{31}^2} \gg |m_2| \approx \sqrt{\Delta m_{31}^2 R_\nu}. \quad (18)$$

B. Inverted Hierarchy

For inverted hierarchy with mass $m_3 = 0$, Eq. (12) can be written as

$$U_{a1}U_{b1} + pU_{a2}U_{b2} + qU_{a4}U_{b4}e^{2i\delta_{14}} = 0, \quad (19)$$

where $p = \frac{m_2}{m_1}e^{2i\alpha}$ and $q = \frac{m_4}{m_1}e^{2i\gamma}$. Solving Eq. (19) gives

$$p = - \left(\frac{U_{a1}U_{b1} + qU_{a4}U_{b4}e^{2i\delta_{14}}}{U_{a2}U_{b2}} \right). \quad (20)$$

We can extract the neutrino mass ratio as

$$\frac{m_2}{m_1} = |p|$$

and one of the Majorana phases is found to be

$$\alpha = \frac{1}{2} \arg(p). \quad (21)$$

Here the physical Majorana phases are α and γ . For inverted hierarchy the remaining three neutrino masses are given as $m_1 = \sqrt{\Delta m_{31}^2}$, $m_2 = \sqrt{\Delta m_{21}^2 + \Delta m_{31}^2}$ and $m_4 = \sqrt{\Delta m_{43}^2}$. We define the two independent neutrino mass squared difference ratios as,

$$\begin{aligned} R_\nu &= \frac{\Delta m_{21}^2}{\Delta m_{31}^2} = |p|^2 - 1, \\ R_{\nu_1} &= \frac{\Delta m_{43}^2}{\Delta m_{31}^2} = |q|^2, \end{aligned} \quad (22)$$

where $|q| = \frac{m_4}{m_1}$. The allowed 3σ ranges of these two mass ratios calculated from the experimental data are

$$\begin{aligned} R_\nu &= (2.7 \times 10^{-2} - 3.7 \times 10^{-2}), \\ R_{\nu_1} &= (0.27 \times 10^3 - 1.14 \times 10^3) \end{aligned} \quad (23)$$

For the case of IH with $m_3 = 0$ and using $R_\nu \ll 1$ the masses can be written in terms of R_{ν_1} as

$$\text{SIH} : |m_4| \approx \sqrt{\Delta m_{31}^2 R_{\nu_1}} \gg |m_2| \approx \sqrt{(1 + R_\nu) \Delta m_{31}^2} \approx \sqrt{\Delta m_{31}^2} \approx |m_1| \approx \sqrt{\Delta m_{31}^2}. \quad (24)$$

C. Quasidegenerate Mass Spectrum

For quasidegenerate mass spectrum the three active neutrinos have approximately same mass and are lighter compared

to the mass of sterile neutrino,

$$QD : |m_4| \gg |m_1| \approx |m_2| \approx |m_3| \approx m_0. \quad (25)$$

Using QD approximation the one-zero texture equation (Eq. (12)) can be written as,

$$m_0(U_{a1}U_{b1} + U_{a2}U_{b2}e^{2i\alpha} + U_{a3}U_{b3}e^{2i(\beta+\delta_{13})}) + m_4U_{a4}U_{b4}e^{2i(\gamma+\delta_{14})} = 0$$

In the QD regime we vary m_0 from 0.1 eV - 0.3 eV.

IV. RESULTS

In this section we first study the implications of a vanishing element $M_{\alpha\beta}$ with vanishing lowest mass for the 3+1 scenario, where $\alpha, \beta = e, \mu, \tau, s$ and then study the implications of quasidegenerate neutrino mass spectrum in the active sterile mixing. The vanishing lowest neutrino mass in addition to the zero texture have non-trivial implications and results in the constrained parameter space of neutrino masses and CP violating phases. Interesting parameters correlations are also obtained for the quasidegenerate case. Since $M_{\alpha\beta}$ is complex the above condition implies both real and imaginary parts are zero. Therefore to study the one-zero textures we consider $|M_{\alpha\beta}| = 0$.

A. The mass matrix element M_{ee}

The matrix element M_{ee} in the 3+1 scenario is given as,

$$M_{ee} = m_1c_{14}^2c_{13}^2c_{12}^2 + m_2s_{12}^2c_{14}^2c_{13}^2e^{2i\alpha} + m_3s_{13}^2c_{14}^2e^{2i\beta} + m_4s_{14}^2e^{2i\gamma}. \quad (27)$$

The 3+1 picture have predictions that are completely different from standard 3 active scenario. M_{ee} cannot vanish in 3 active scenario if the lowest mass vanishes [29, 43]. In 3+1 case we find that it can vanish due to the contribution from the sterile sector. The contribution of the sterile neutrino to the element M_{ee} comes from the mass m_4 and the active-sterile mixing angle θ_{14} . The mass matrix element M_{ee} has the simplest form because of the chosen parametrization and can be understood quite well.

For NH ($m_1 = 0$) the zero-texture at M_{ee} can be written as,

$$|c_{14}^2(\sqrt{R_\nu}s_{12}^2c_{13}^2e^{2i\alpha} + s_{13}^2e^{2i\beta}) + \sqrt{R_{\nu_1}}s_{14}^2e^{2i\gamma}| = 0. \quad (28)$$

For $\theta_{14} = 0^\circ$ this expression reduces to one-zero texture in 3 active neutrino mixing scenario. In the three active neutrino case for $\beta = 0^\circ$ and $\alpha = +90^\circ$ (which maximizes the cancellation between the terms) M_{ee} predicts

$$s_{13}^2 = \sqrt{R_\nu}s_{12}^2c_{13}^2, \quad (29)$$

which gives $s_{13}^2 = 0.047$ for the lowest value of R_ν and this is higher than the experimental prediction. Thus for three active scenario M_{ee} can not be zero for NH when m_1 is zero [44]. We found earlier in our 3+1 scenario analysis [27] that the cancellation of terms on the RHS of Eq. (28) is possible only if m_1 is large. In our present case since lowest mass is vanishing, the major contribution will come from additional sterile

neutrino because of higher values of m_4 . Even for very small allowed values of θ_{14} the sterile contribution (third term) in Eq. (28) is large and cannot have equal magnitude to the other two terms on its left. Thus, complete cancellation of the terms is never possible resulting in non vanishing M_{ee} for NH. The only possible way to have vanishing M_{ee} is when θ_{14} is very small. It's typical value can be obtained from Eq. (28) as,

$$\tan^2\theta_{14} = -\frac{s_{13}^2e^{2i\beta} + \sqrt{R_\nu}s_{12}^2c_{13}^2e^{2i\alpha}}{\sqrt{R_{\nu_1}}e^{2i\gamma}}. \quad (30)$$

Substituting $\alpha = \beta = 0^\circ$ (which would maximize the active neutrino contribution) and $\gamma = +90^\circ$ we get $\tan^2\theta_{14} \approx 10^{-3}$ i.e., θ_{14} lies well outside its allowed 3σ range and is thus not allowed.

For IH when $m_3 = 0$, zero texture condition for M_{ee} can be written as,

$$|c_{14}^2c_{13}^2(c_{12}^2 + s_{12}^2e^{2i\alpha}) + \sqrt{R_{\nu_1}}s_{14}^2e^{2i\gamma}| = 0. \quad (31)$$

As can be seen from above equation the magnitude of M_{ee} for IH depends on α and γ along with the mixing angles. For IH the complete cancellation is never possible in three active neutrino scenario because in addition to $\alpha = +90^\circ$ cancellation requires $s_{12}^2 = c_{12}^2$ [29, 43]. These results change when we include the sterile contribution. The element M_{ee} vanishes for IH in the limit $m_3 \approx 0$ when $\alpha = 0^\circ$ and $\gamma = +90^\circ$ provided

$$\tan^2\theta_{14} \approx \frac{c_{13}^2}{\sqrt{R_{\nu_1}}} \approx 0.05 \quad (32)$$

which is well within the allowed range. This behaviour is in stark contrast to that of the 3 neutrino case [43]. Note that, by considering vanishing lowest mass, the other two masses are highly constrained in the present scenario. $m_1 = \sqrt{\Delta m_{31}^2}$ and $m_2 = \sqrt{\Delta m_{31}^2 + \Delta m_{21}^2}$ for IH. From Eq. (31) it is evident that the cancellation of all three terms are dependent on the two Majorana phases α and γ . The order of magnitude of each term is approximately the same of the order of $\mathcal{O}(10^{-2})$. The cancellation of these terms are only possible for constrained values of Majorana phase γ (around $+90^\circ$) as shown in the upper left panel of Fig. (2). Note that as m_4 is large compared to m_1 and m_2 , for cancellation between the active and sterile sector, one expects to have lower values of s_{14}^2 for high m_4 values. This is evident from the upper right panel of Fig. (2) where we can see that the higher values of θ_{14} are disallowed as the value of m_4 increases.

The matrix element M_{ee} for QD neutrino masses is given as,

$$M_{ee} = m_0c_{14}^2c_{13}^2(c_{12}^2 + s_{12}^2e^{2i\alpha}) + m_0s_{13}^2c_{14}^2e^{2i\beta} + m_4s_{14}^2e^{2i\gamma}. \quad (33)$$

The correlation plots for QD mass spectrum when M_{ee} vanishes are given in the lower panels of Fig. (2). We observe that unlike the completely hierarchical mass spectrum (upper left panel of Fig. (2)), here, the phase α is also constrained. For $\alpha = 0^\circ$ or 180° and $\beta = 0^\circ$ the above expression reduces to

$$M_{ee} = m_0c_{14}^2 + m_4s_{14}^2e^{2i\gamma}. \quad (34)$$

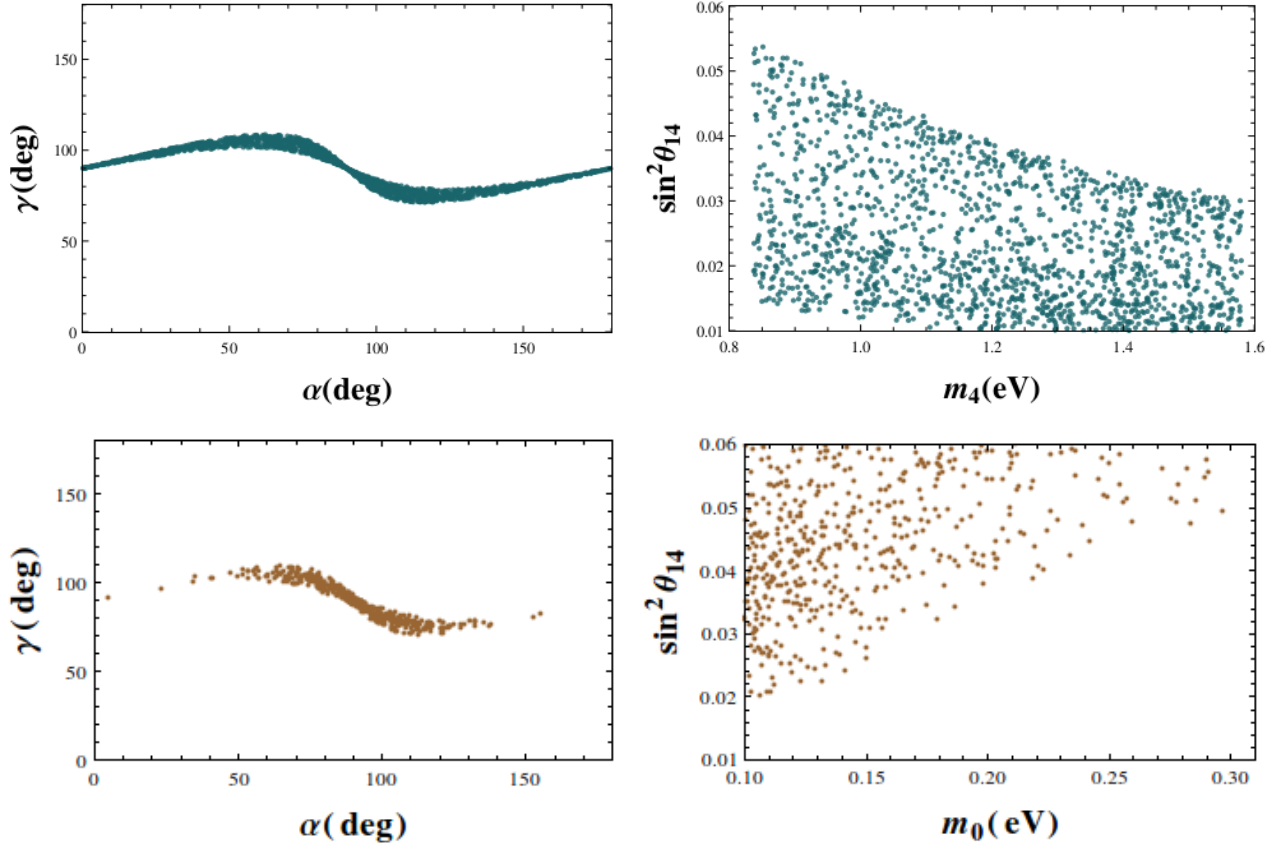


FIG. 2. Correlation plots for $|M_{ee}| = 0$, IH (upper panel) and quasidegeneracy (lower panel).

When $\gamma \sim 90^\circ$ the term $m_0 c_{14}^2$ becomes order of magnitude greater than the second term and hence the cancellation of these two terms becomes impossible. We see this behavior in the $(\alpha - \gamma)$ plot in the lower left panel of Fig. (2) where $\alpha = 0^\circ$ or 180° is disallowed. However, when $\alpha = \beta = \gamma = 90^\circ$, Eq. (33) becomes

$$M_{ee} = m_0 c_{14}^2 (c_{13}^2 \cos 2\theta_{12} - s_{13}^2) - m_4 s_{14}^2. \quad (35)$$

Now all terms in the above expression are of same order. Thus M_{ee} can vanish for these values of Majorana phases α and γ . Note that the other phase β is unconstrained here. From the above expressions it is clear that vanishing of M_{ee} for QD mass spectrum depends on active sterile mixing angle θ_{14}

along with the Majorana phases α and γ . In the lower right panel of Fig. (2), we plot $\sin^2 \theta_{14}$ as a function of m_0 . As m_0 increases, θ_{14} constrains to higher values. This behaviour can also be understood from Eq (35). As the active neutrino mass increases, higher values of θ_{14} are needed to allow cancellation between the active and the sterile terms.

B. The mass matrix elements $M_{e\mu}$ and $M_{e\tau}$

The mass matrix element $M_{e\mu}$ in the 3+1 scenario is given as,

$$\begin{aligned} M_{e\mu} = & m_4 c_{14} (e^{i(\delta_{14} - \delta_{24} + 2\gamma)} s_{14} s_{24} + m_3 e^{i(\delta_{13} + 2\beta)} s_{13} (c_{13} c_{24} s_{23} - e^{i(\delta_{14} - \delta_{13} - \delta_{24})} s_{13} s_{14} s_{24})) \\ & + m_1 c_{12} c_{13} (-c_{23} c_{24} s_{12} + c_{12} (-e^{i\delta_{13}} c_{24} s_{13} s_{23} - e^{i(\delta_{14} - \delta_{24})} c_{13} s_{14} s_{24})) \\ & + m_2 e^{2i\alpha} c_{13} s_{12} (c_{12} c_{23} c_{24} + s_{12} (-e^{i\delta_{13}} c_{24} s_{13} s_{23} - e^{i(\delta_{14} - \delta_{24})} c_{13} s_{14} s_{24})). \end{aligned} \quad (36)$$

This expression is complicated as compared to M_{ee} and thus it becomes impossible to study the behaviour of independent

parameters. To simplify this expressions we introduce a small parameter $\lambda \equiv 0.2$ and retain terms of the order of λ^2 . We

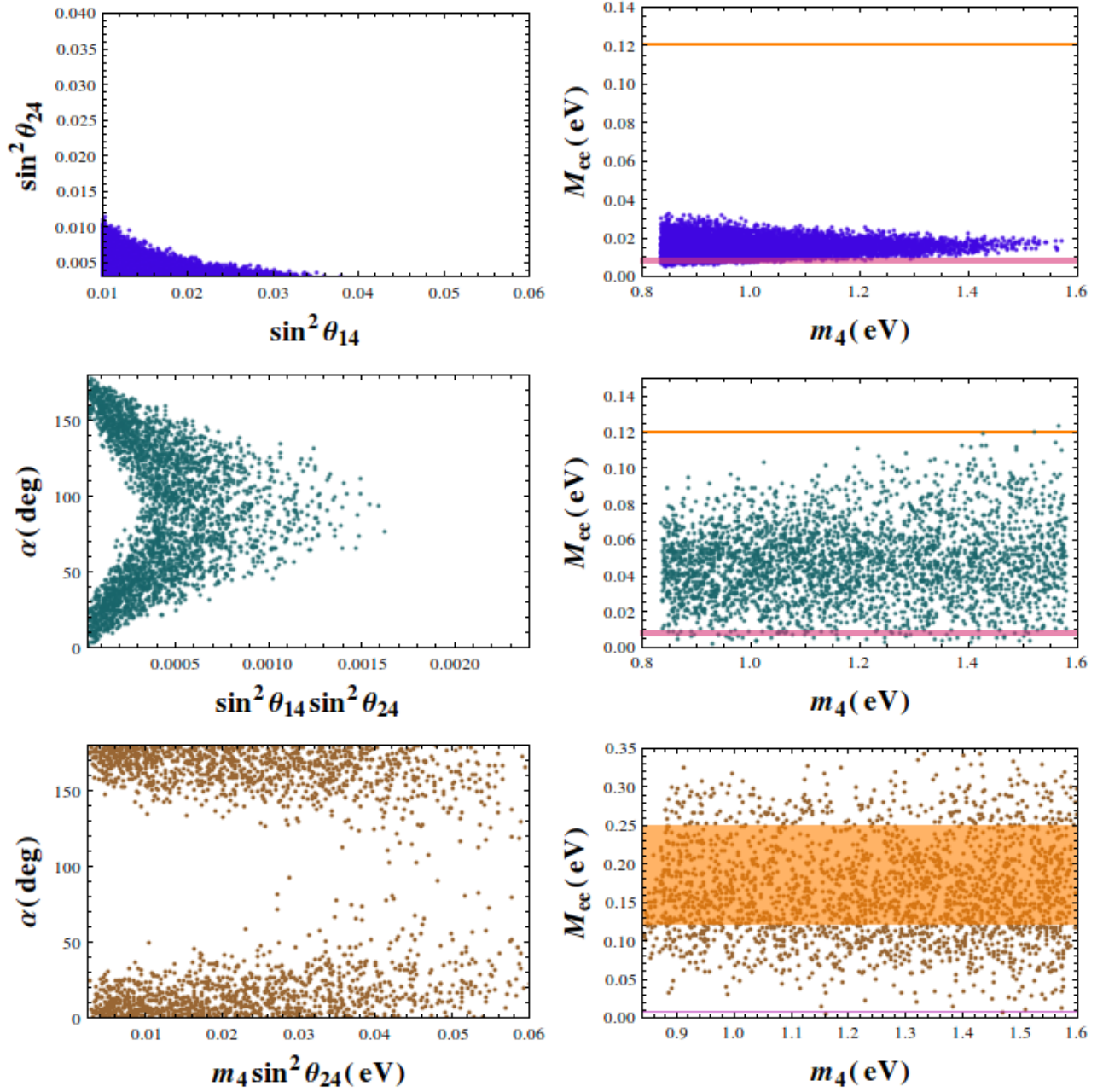


FIG. 3. Correlation plots for $|M_{e\mu}| = 0$. Upper (middle) row is for NH (IH) and lower row is for QD mass spectrum. Orange line in the upper and middle right panels represent the lowest value of the upper bound on M_{ee} from KamLAND-ZEN + EXO-200. The purple line is the sensitivity from next generation experiments [42]. The orange band in the lower right panel represents the full allowed range of M_{ee} from combined results of KamLAND-ZEN and EXO-200.

define the small angles θ_{14} , θ_{24} and θ_{13} in the form $a\lambda$.

$$\begin{aligned} \sin\theta_{14} &\approx \theta_{14} \equiv a_{14}\lambda, \\ \sin\theta_{24} &\approx \theta_{24} \equiv a_{24}\lambda, \\ \sin\theta_{13} &\approx \theta_{13} \equiv a_{13}\lambda, \end{aligned} \quad (37)$$

where a_{ij} are parameters of $\mathcal{O}(1)$ and their 3σ range from the current constraint on the mixing angles is given by

$$\begin{aligned} a_{13} &= 0.68 - 0.81, \\ a_{14} &= 0.5 - 1.2, \\ a_{24} &= 0.25 - 1. \end{aligned} \quad (38)$$

Note that the sterile mixing angle θ_{34} can be large (has an upper bound) and thus we do not approximate this angle. We will use the above approximations to understand the behaviour of different parameters wherever required.

The condition of zero texture at $M_{e\mu}$ for NH with vanishing lowest mass ($m_1 = 0$) gives,

$$\begin{aligned} & |m_4 c_{14} (e^{i(\delta_{14}-\delta_{24}+2\gamma)} s_{14} s_{24} \\ & + m_3 e^{i(\delta_{13}+2\beta)} s_{13} (c_{13} c_{24} s_{23} - e^{i(\delta_{14}-\delta_{13}-\delta_{24})} s_{13} s_{14} s_{24}) \\ & + m_2 e^{2i\alpha} c_{13} s_{12} (c_{12} c_{23} c_{24} \\ & + s_{12} (-e^{i\delta_{13}} c_{24} s_{13} s_{23} - e^{i(\delta_{14}-\delta_{24})} c_{13} s_{14} s_{24})))| = 0. \end{aligned} \quad (39)$$

From the above expression we see that the sterile sector contribution appears as θ_{14} and θ_{24} . For cancellation of sterile term with the active part, the values of these angles must be small. This is clear from the upper left panel of Fig. (3) where we give the correlation of s_{14}^2 with s_{24}^2 . We see that the higher values of s_{14}^2 and s_{24}^2 are disallowed and as s_{14}^2 increases, s_{24}^2 decreases. In the upper right panel of Fig. (3) we give the prediction for the effective mass M_{ee} as a function of m_4 . As M_{ee} is proportional to $s_{14}^2 m_4$ it is expected that as m_4 increases, one should get higher values of effective Majorana mass. But in this particular case we do not see this feature. This is because for cancellation to occur between the active and sterile terms in $M_{e\mu}$, one needs smaller θ_{14} for the higher values of m_4 and thus higher values of M_{ee} are not possible even when m_4 is large. Thus, for NH and $|M_{e\mu}| = 0$ there exists an upper bound on effective mass $M_{ee} < 0.04$ eV.

The zero texture at $M_{e\mu}$ for IH with vanishing lowest mass ($m_3 = 0$) in 3+1 scenario using approximations given in Eqs. (24, 37) can be written as,

$$\begin{aligned} & |c_{12} s_{12} c_{23} (e^{2i\alpha} - 1) \\ & - s_{23} a_{13} e^{i\delta_{13}} (c_{12}^2 + s_{12}^2 e^{2i\alpha}) \lambda \\ & - e^{i(\delta_{14}-\delta_{24})} a_{14} a_{24} (c_{12}^2 - e^{2i\gamma} \sqrt{R_{\nu 1}} + e^{2i\alpha} s_{12}^2) \lambda^2| = 0, \end{aligned} \quad (40)$$

which is independent of θ_{34} and Majorana phase β .

From the above equation it can be noted that for $\alpha = 0^\circ$, the leading order term vanishes. Thus for cancellation to occur one needs very small values of θ_{14} and θ_{24} which appears with the large m_4 term. On the other hand when α is $+90^\circ$, the leading order term is very large and one requires higher values of the above mentioned mixing angles for cancellation. This is shown in the middle left panel of Fig. (3). Here, for $\alpha = 0^\circ$, the allowed values of $\sin^2 \theta_{14} \sin^2 \theta_{24}$ are very small and on the contrary, for $\alpha = +90^\circ$ the smaller values of $\sin^2 \theta_{14} \sin^2 \theta_{24}$ are disallowed. Here the upper bound of effective mass M_{ee} can be as high as 0.13 eV (middle right panel of Fig. (3)).

In these figures (as well as for the other allowed textures) we also show the present lowest value of the upper bound on M_{ee} by the orange line and the future expected sensitivity by the purple line. These figures clearly show that the values of M_{ee} are always lower than the present bound on M_{ee} for NH. Whereas for IH, values of M_{ee} are below the current bound for smaller value of m_4 but for higher value of m_4 there are a few points of M_{ee} which are above the lowest value of the current upper bound i.e., above the orange line. The above

statement is also true for all the M_{ee} figures for completely hierarchical mass presented in the subsequent sections. Using approximations given in Eq.(25, 37) for quasidegeneracy, the zero texture at $M_{e\mu}$ for QD spectrum can be written as,

$$\begin{aligned} & |m_0 [c_{12} s_{12} c_{23} (e^{2i\alpha} - 1) \\ & + a_{13} s_{23} e^{i\delta_{13}} (-c_{12}^2 + e^{2i\beta} - s_{12}^2 e^{2i\alpha}) \lambda] \\ & - a_{14} a_{24} e^{i\delta_{14}} (c_{12}^2 m_0 - e^{2i\gamma} m_4 + e^{2i\alpha} s_{12}^2 m_0) \lambda^2| = 0. \end{aligned} \quad (41)$$

The correlation plots for the parameters here are given in the lower panels of Fig. (3). The Majorana phase α is largely constrained (values near 0° or 180° are seems to be allowed) for smaller values of $m_4 \sin^2 \theta_{24}$. For larger values of $m_4 \sin^2 \theta_{24}$ this texture is marginally allowed. To understand this behaviour, we consider $\alpha = 90^\circ$ and all other phases to be 0° and express Eq. (41) as,

$$\begin{aligned} & |m_0 [-2(c_{12} c_{23} s_{12}) + 2a_{13} s_{12}^2 s_{23} \lambda] \\ & + (a_{14} a_{24} [m_4 - \cos 2\theta_{12} m_0]) \lambda^2| = 0. \end{aligned} \quad (42)$$

From the equation it is clear that, the $m_4 a_{24}$ term with a coefficient λ^2 (which is small), can only be of the similar order with the leading order m_0 term, when m_4 and θ_{24} is large. Thus for smaller values of $m_4 s_{24}^2$ it is not possible to have any cancellation and thus there are no viable points around $\alpha = 90^\circ$ as seen in the lower left panel of Fig. (3).

However, for $\alpha = 0^\circ$ or 180° , the leading order m_0 term and the subleading term with λ can vanish due to the presence of $(e^{2i\alpha} - 1)$ term. For this reason one can always have cancellation within the remaining λ^2 terms, for all the values of m_4 and s_{24} (lower left panel of Fig. (3)).

In the lower right panel of Fig. (3), we plot the effective Majorana mass M_{ee} vs m_4 . The orange band in this plot, corresponds to the allowed range of M_{ee} with the nuclear matrix element uncertainty as given by the combined analysis of KamLAND-ZEN and EXO-200 (Xe^{136}). From this plot we observe that a certain region of the allowed parameter space can be completely discarded based on the present bound on M_{ee} . However, this is not the case for completely hierarchical neutrino masses. For NH, the allowed values are well below of the current upper limits of M_{ee} and for IH, there are few points which fall in the region of uncertainty i.e., points above the orange line. The conclusion drawn in this section is also true for the next subsequent sections and that can be seen from the right panel figure of each allowed texture.

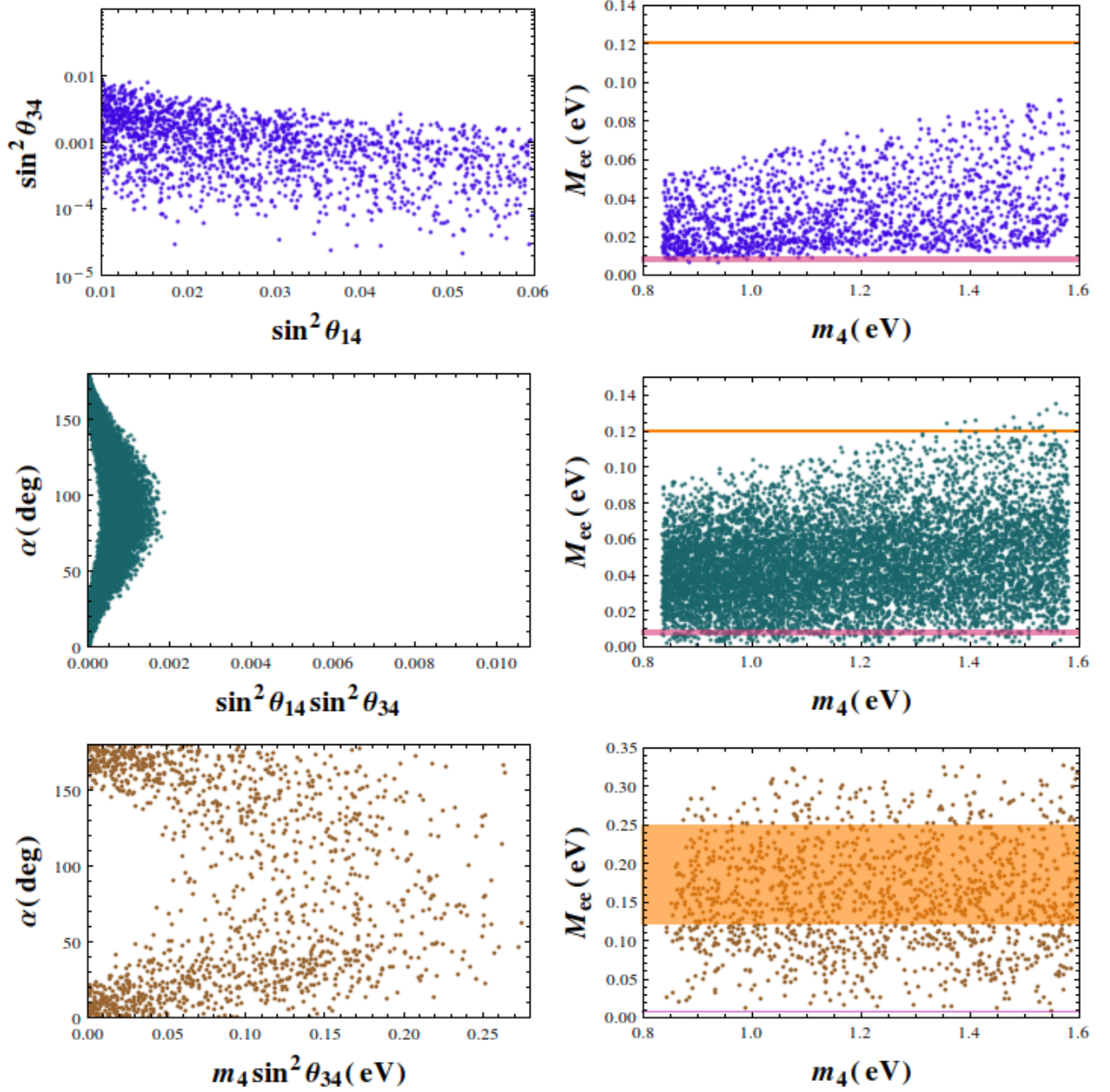


FIG. 4. Correlation plots for $|M_{e\tau}| = 0$ for NH (upper panel), IH (middle panel) and QD (lower panel) mass spectrum. Bounds on M_{ee} are described in the caption of Fig.(3).

The mass matrix element $M_{e\tau}$ in the 3+1 mixing scenario is given as,

$$\begin{aligned}
 M_{e\tau} = & c_{14}c_{24}e^{i(2\gamma+\delta_{14})}m_4s_{14}s_{34} \\
 & + m_3c_{14}s_{13}e^{i(2\beta+\delta_{13})}(-c_{24}s_{13}s_{14}s_{34}e^{i(\delta_{14}-\delta_{13})} \\
 & + c_{13}(c_{23}c_{34} - e^{i\delta_{24}}s_{23}s_{24}s_{34})) \\
 & + m_2s_{12}c_{13}c_{14}e^{2i\alpha}(c_{12}(-c_{34}s_{23} - c_{23}s_{24}s_{34}e^{i\delta_{24}}) \\
 & + s_{12}(-c_{13}c_{24}s_{14}s_{34}e^{i\delta_{14}} \\
 & - e^{i\delta_{13}}s_{13}(c_{23}c_{34} - e^{i\delta_{24}}s_{23}s_{24}s_{34}))) \\
 & + m_1c_{12}c_{13}c_{14}(-s_{12}(-c_{34}s_{23} - c_{23}s_{24}s_{34}e^{i\delta_{24}}) \\
 & + c_{12}(-c_{13}c_{24}s_{14}s_{34}e^{i\delta_{14}} - e^{i\delta_{13}}s_{13} \\
 & (c_{23}c_{34} - e^{i\delta_{24}}s_{23}s_{24}s_{34}))).
 \end{aligned} \tag{43}$$

The two elements $M_{e\mu}$ and $M_{e\tau}$ in 3 active neutrino scenario are related by $\mu - \tau$ permutation symmetry [45–48]. Here in 3+1 case also these two elements are related as

$$(M_\nu)_{e\tau} = P_{\mu\tau}^T (M_\nu)_{e\mu} P_{\mu\tau}.$$

where permutation matrix $P_{\mu\tau}$ is given as

$$P_{\mu\tau} = \begin{pmatrix} 1 & 0 & 0 & 0 \\ 0 & 0 & 1 & 0 \\ 0 & 1 & 0 & 0 \\ 0 & 0 & 0 & 1 \end{pmatrix}.$$

For three active neutrino case the atmospheric mixing angle θ_{23} in the $\mu - \tau$ symmetric textures are related as $\bar{\theta}_{23} = (\frac{\pi}{2} - \theta_{23})$. However, in the 3+1 case the relation of θ_{23} between two texture structures related by this symmetry is not simple [26]. The active sterile mixing angles θ_{24} and θ_{34} are also different and are related as,

$$\bar{\theta}_{12} = \theta_{12}, \quad \bar{\theta}_{13} = \theta_{13}, \quad \bar{\theta}_{14} = \theta_{14}, \quad (44)$$

$$\sin \bar{\theta}_{24} = \sin \theta_{34} \cos \theta_{24} \quad (45)$$

$$\sin \bar{\theta}_{23} = \frac{\cos \theta_{23} \cos \theta_{34} - \sin \theta_{23} \sin \theta_{34} \sin \theta_{24}}{\sqrt{1 - \cos \theta_{24}^2 \sin \theta_{34}^2}} \quad (46)$$

$$\sin \bar{\theta}_{34} = \frac{\sin \theta_{24}}{\sqrt{1 - \cos \theta_{24}^2 \sin \theta_{34}^2}}. \quad (47)$$

Due to these complex relations the behaviour of $M_{e\mu}$ is different from that of $M_{e\tau}$ unlike in three active neutrino case where the plots of these two elements were same except for θ_{23} which differed in octant for both the textures.

It is found that in the limit of small θ_{24} the two active sterile mixing angles $\bar{\theta}_{24} \approx \theta_{34}$ from Eq. (45). The same can be seen from Eq. (47) which gives $\bar{\theta}_{34} \approx \theta_{24}$ for smaller values of the mixing angle θ_{34} . Thus, for small θ_{24} and θ_{34} , the behaviour shown by θ_{24} in $M_{e\mu}$ ($M_{\mu\mu}$) is same as shown by θ_{34} in $M_{e\tau}$ ($M_{\tau\tau}$).

In Fig. (4) we have have plotted the correlation plots for $|M_{e\tau}| = 0$. The upper panels are for NH and middle panels are for IH. As discussed above, from the plots we see that the properties shown by s_{24}^2 in $M_{e\mu}$ are similar for s_{34}^2 in this case. Here we can see that for NH, the allowed values of s_{34}^2 are very small. Unlike $M_{e\mu}$, here s_{14}^2 is allowed in its complete 3σ range. As there is no lower limit on θ_{34} , it can be extremely small (of the order of 10^{-4}) even when s_{14}^2 is large to give allowed texture. For IH, the result is also similar to that of $M_{e\mu}$, where we can see that for $\alpha = 0^\circ$, the higher values of $s_{14}^2 s_{34}^2$ are not preferred and for $\alpha = +90^\circ$, the very low values of $s_{14}^2 s_{34}^2$ are not allowed. We also notice that the values of $s_{14}^2 s_{34}^2$ are restricted within 0.002 which is of the same order in magnitude as obtained for $s_{14}^2 s_{24}^2$ in $M_{e\mu}$. The bounds for the effective mass M_{ee} are obtained as < 0.09 eV for NH and < 0.14 eV for IH.

In the lower panels of Fig. (4), we give the correlation plots for $M_{e\tau}$ for quasidegenerate mass spectrum. As mentioned above, the behaviour of this texture is related to $M_{e\mu}$ by the $\mu - \tau$ permutation symmetry. From the lower left pane of Fig. (4), we see that the nature of correlation for $(m_4 \sin^2 \theta_{34})$ in $|M_{e\tau}| = 0$, is exactly same as that of $(m_4 \sin^2 \theta_{24})$ in $|M_{e\mu}| = 0$ (lower left panel of Fig. (3)).

C. The mass matrix elements $M_{\mu\mu}$ and $M_{\tau\tau}$

The (2,2) diagonal matrix element in the 3+1 scenario is given as,

$$\begin{aligned} M_{\mu\mu} = & e^{2i(\delta_{14}-\delta_{24}+\gamma)} c_{14}^2 m_4 s_{24}^2 \\ & + e^{2i(\delta_{13}+\beta)} m_3 (c_{13} c_{24} s_{23} \\ & - e^{i(\delta_{14}-\delta_{13}-\delta_{24})} s_{13} s_{14} s_{24})^2 + m_1 \{-c_{23} c_{24} s_{12} \\ & + c_{12} (-e^{i\delta_{13}} c_{24} s_{13} s_{23} - e^{i(\delta_{14}-\delta_{24})} c_{13} s_{14} s_{24})\}^2 \\ & + e^{2i\alpha} m_2 \{c_{12} c_{23} c_{24} \\ & + s_{12} (-e^{i\delta_{13}} c_{24} s_{13} s_{23} - e^{i(\delta_{14}-\delta_{24})} c_{13} s_{14} s_{24})\}^2. \end{aligned} \quad (48)$$

For NH, considering lowest vanishing mass ($m_1 = 0$), using the approximations as defined in Eqs. (18, 37) and putting the Majorana phases equal to zero as well as the Dirac phases equal to 180° , the zero texture condition yields:

$$\begin{aligned} & s_{23}^2 + c_{12}^2 c_{23}^2 \sqrt{R_\nu} + c_{12} s_{12} \sin 2\theta_{23} \sqrt{R_\nu} \lambda a_{13} \\ & + \lambda^2 (s_{12}^2 s_{23}^2 \sqrt{R_\nu} a_{13}^2 - c_{23} \sin 2\theta_{12} \sqrt{R_\nu} a_{14} a_{24} \\ & + \sqrt{R_\nu} a_{24}^2) = 0. \end{aligned} \quad (49)$$

From the expression we can understand that when θ_{24} is small, the leading order terms become larger as compared to the $R_{\nu 1}$ term. On the other hand when θ_{24} is very large, the $R_{\nu 1}$ becomes larger than the leading order terms. Thus it will not be possible to have $|M_{\mu\mu}| = 0$ in NH for either very small or very large values of θ_{24} . This is evident from the upper left panel of Fig. (5). Here we can see that though s_{14}^2 is allowed in its 3σ range but the smaller as well as higher values of θ_{24} are disallowed. In this case the effective mass M_{ee} is always less than 0.10 eV (upper right panel of Fig. 5).

For IH and $m_3 = 0$, using the approximations as defined in Eqs. (24, 37) the expression for $M_{\mu\mu}$ becomes:

$$\begin{aligned} M_{\mu\mu} \approx & c_{23}^2 (s_{12}^2 + c_{12}^2 e^{2i\alpha}) \\ & + \frac{1}{2} \lambda \sin 2\theta_{12} \sin 2\theta_{23} e^{i\delta_{13}} (1 - e^{2i\alpha}) a_{13} \\ & + \lambda^2 [\sin 2\theta_{12} c_{23} e^{i(\delta_{14}-\delta_{24})} (1 - e^{2i\alpha}) a_{14} a_{24} \\ & + s_{23}^2 e^{2i\delta_{13}} (c_{12}^2 + e^{2i\alpha} s_{12}^2) a_{13}^2 \\ & + e^{2i(\gamma+\delta_{14}-\delta_{24})} \sqrt{R_{\nu 1}} a_{24}^2]. \end{aligned} \quad (50)$$

Further putting the phase $\alpha = 0^\circ$ and $\theta_{24} = 0^\circ$, the above equation simplifies to

$$M_{\mu\mu} \approx c_{23}^2 + s_{23}^2 s_{13}^2 e^{2i\delta_{13}} \quad (51)$$

Thus $M_{\mu\mu}$ can not vanish for IH when the phase α is zero and θ_{24} is small. But for the higher values of θ_{24} the $R_{\nu 1}$ term will start contributing and it becomes possible to have cancellation even if $\alpha = 0^\circ$. On the other hand when $\alpha = +90^\circ$, the contributions of the λ and λ^2 terms come into play and thus one can have cancellations for the smaller values of θ_{24} . This can be seen from the left middle panel of Fig. (5) where we can see that at $\alpha = 0^\circ$, the smaller values of s_{24}^2 are disallowed and at $\alpha = +90^\circ$ the values less than 0.022 of s_{24}^2 are allowed. In this case the upper bound of the effective mass is 0.14 eV as seen from the right middle panel of Fig. (5). In the

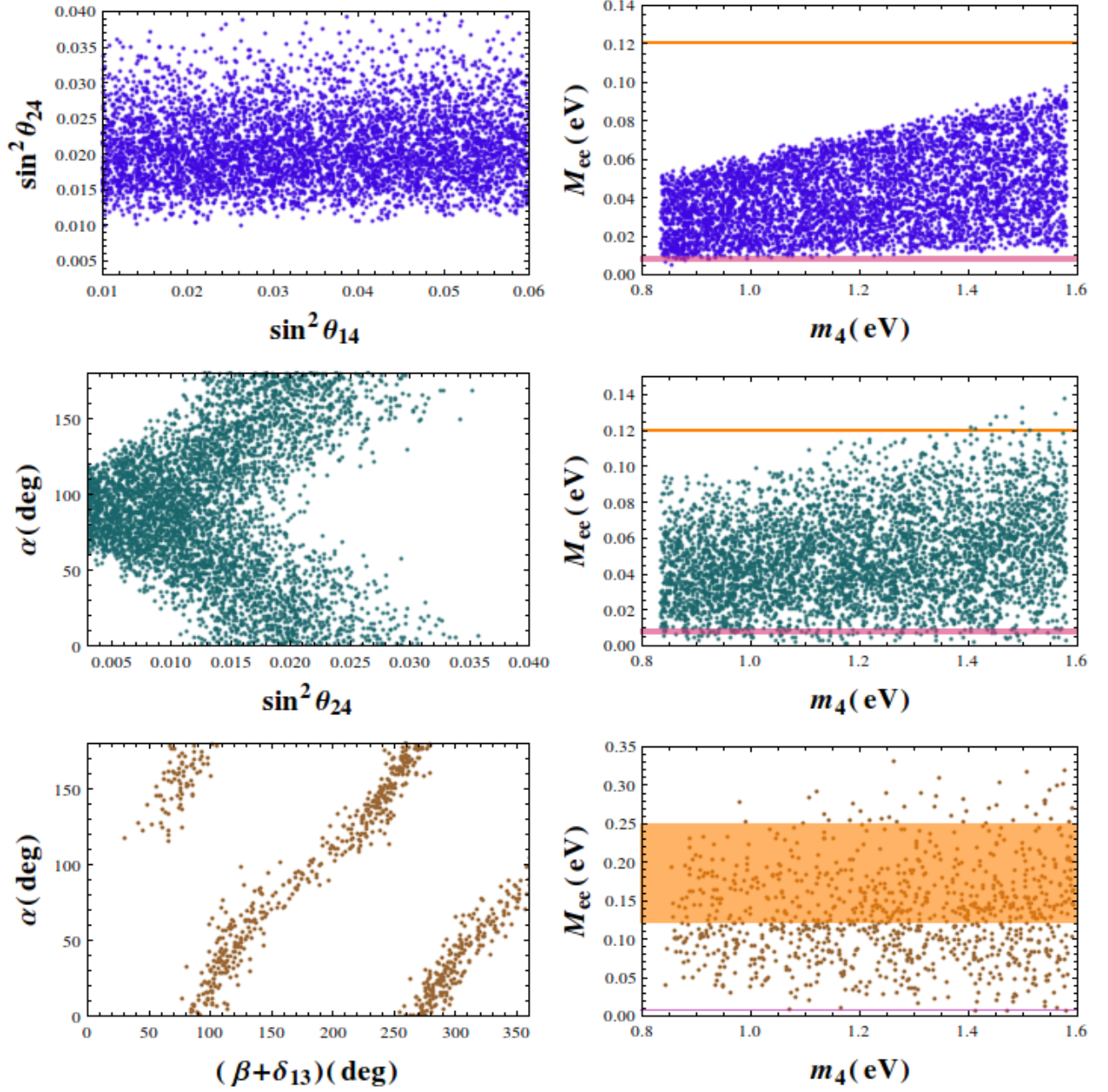


FIG. 5. Correlation plots for $|M_{\mu\mu}| = 0$ for NH (upper panel), IH (middle panel) and QD (lower panel) mass spectrum. Bounds on M_{ee} are described in the caption of Fig.(3).

lower panels of Fig. (5), we have given the correlation plots of $|M_{\mu\mu}| = 0$ for QD mass spectrum. To understand these correlations, we have expanded Eq. (48) using the approximations as given in Eqs. (37) and (25) to obtain the following:

$$|(c_{12}^2 c_{23}^2 e^{2i\alpha} + c_{23}^2 s_{12}^2 + e^{2i(\beta+\delta_{13})} s_{23}^2) m_0 - 2(a_{13} c_{12} c_{23} e^{i\delta_{13}} (e^{2i\alpha} - 1) m_0 s_{12} s_{23}) \lambda + \mathcal{O}(\lambda^2)| = 0. \quad (52)$$

In this case we note that, unlike the textures $|M_{e\mu}| = 0$ and

$|M_{e\tau}| = 0$, the factor $(e^{2i\alpha} - 1)$ appears with the subleading λ term and the leading order term contains the $(\beta + \delta_{13})$ factor. For the values $\alpha = 0^\circ$ and $(\beta + \delta_{13}) = 90^\circ$, the survived terms of Eq. (52) are $(m_0 \cos 2\theta_{23})$ and the subleading λ^2 term. As both the terms have the magnitude of the order of $\mathcal{O}(10^{-2})$, there can be cancellation of these terms leading to the possibility of vanishing $M_{\mu\mu}$. However, for $\alpha = 90^\circ$ and $(\beta + \delta_{13}) = 90^\circ$, the magnitude of the leading order term

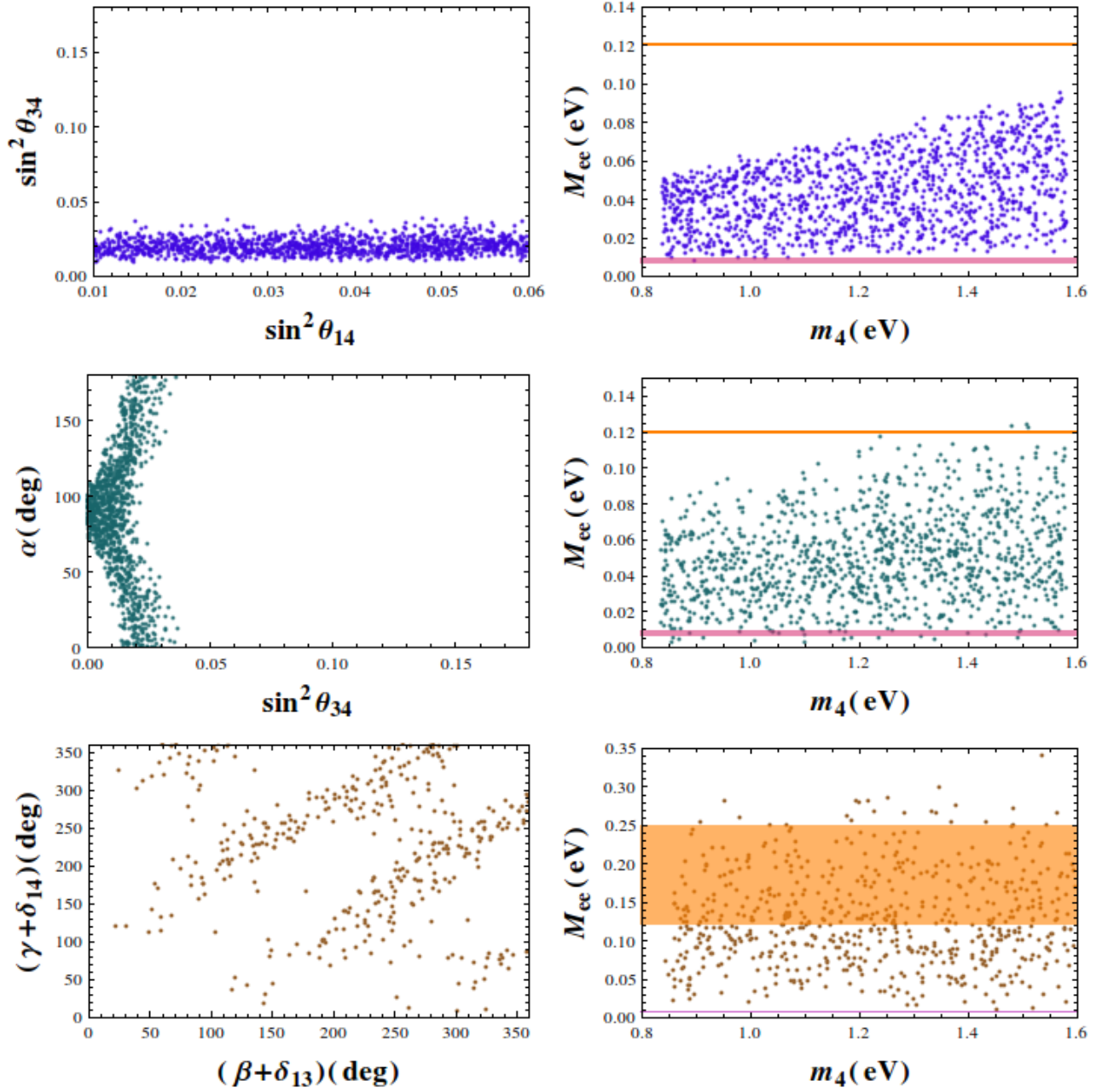


FIG. 6. Correlation plots for $|M_{\tau\tau}| = 0$ for NH (upper panel), IH (middle panel) and QD (lower panel) mass spectrum. Bounds on M_{ee} are described in the caption of Fig.(3).

$(m_0[-c_{23}^2 \cos 2\theta_{12}s_{23}^2])$ is large ($\mathcal{O}(10^{-1})$) than the subleading terms having coefficient λ and λ^2 . Thus one can not have cancellation at these values of α and $(\beta + \delta_{13})$. These conclusions are clearly reflected in the lower left panel of Fig. (5), where we have plotted α as a function of $(\beta + \delta_{13})$.

The mass matrix element $M_{\tau\tau}$ in the 3+1 mixing scenario

is given as,

$$\begin{aligned}
 M_{\tau\tau} = & m_4 e^{2i(\delta_{14} + \gamma)} c_{14}^2 c_{24}^2 s_{34}^2 \\
 & + m_3 e^{2i(\delta_{13} + \beta)} \{ e^{i(\delta_{14} - \delta_{13})} c_{24} s_{13} s_{14} s_{34} \\
 & + c_{13} (c_{23} c_{34} - e^{i\delta_{24}} s_{23} s_{24} s_{34}) \}^2 \\
 & + m_1 [-s_{12} (-c_{34} s_{23} - e^{i\delta_{24}} c_{23} s_{24} s_{34}) \\
 & + c_{12} \{ -e^{i\delta_{14}} c_{13} c_{24} s_{14} s_{34} - e^{i\delta_{13}} s_{13} (c_{23} c_{34} \\
 & - e^{i\delta_{24}} s_{23} s_{24} s_{34}) \}]^2 \\
 & + e^{2i\alpha} m_2 [c_{12} (-c_{34} s_{23} - e^{i\delta_{24}} c_{23} s_{24} s_{34}) \\
 & + s_{12} \{ -e^{i\delta_{14}} c_{13} c_{24} s_{14} s_{34} - e^{i\delta_{13}} s_{13} (c_{23} c_{34} \\
 & - e^{i\delta_{24}} s_{23} s_{24} s_{34}) \}]^2
 \end{aligned} \tag{53}$$

As $M_{\tau\tau}$ is related to $M_{\mu\mu}$ by $\mu - \tau$ symmetry, the behaviour of θ_{34} in $M_{\tau\tau}$ is similar to θ_{24} in $M_{\mu\mu}$. This can be seen from the correlation plots for $|M_{\tau\tau}| = 0$ in Fig. (6).

For NH, very low and high values of s_{34}^2 are disallowed (upper left panel of Fig. (6)) and for IH the correlation between the phase α and s_{34}^2 (middle left panel of Fig. (6)) is exactly similar with the α and s_{24}^2 correlation in $M_{\mu\mu}$ and in both the cases s_{24}^2 and s_{34}^2 are restricted to below 0.04. The upper bounds of the effective mass in this case is 0.10 eV (0.14 eV) in NH (IH) as shown in upper (middle) right panel of Fig. (6).

For the QD case, using the approximation as given in Eqs. (25) and (37), Eq. (53) can be simplified as,

$$|m_0(c_{23}^2 c_{34}^2 e^{2i(\beta+\delta_{13})} + (c_{12}^2 e^{2i\alpha} + s_{12}^2) s_{23}^2 c_{34}^2) + e^{2i(\gamma+\delta_{14})} m_4 s_{34}^2) + \mathcal{O}(\lambda) + \mathcal{O}(\lambda^2)| = 0 \quad (54)$$

Here, unlike $M_{\mu\mu}$, the phase factors $(\beta+\delta_{13})$, α^3 and $(\gamma+\delta_{14})$ appear with the leading order m_0 term. From the lower left panel of Fig. (6), we see that in the $((\beta+\delta_{13}), (\gamma+\delta_{14}))$ plane $(0^\circ, 0^\circ)$ point is not allowed. To understand this point, we consider all phases to be zero in Eq. (54) and this gives

$$m_0 + (m_4 - m_0) s_{34}^2 + (a_{14}^2 + a_{24}^2)(m_0 - m_4) s_{34}^2 \lambda^2 = 0 \quad (55)$$

Here we can see that the above equation is free from the λ term. Thus cancellation between leading order term ($\mathcal{O}(10^{-1})$) and λ^2 term ($\mathcal{O}(10^{-2})$) is not possible for any values of the remaining oscillation parameters. Whereas, for other allowed values of phases, for example: $(\beta+\delta_{13}) = 250^\circ$ and $(\gamma+\delta_{14}) = 150^\circ$, the figure shows that one can have $|M_{\tau\tau}| = 0$ for quasidegenerate mass spectrum.

D. The mass matrix elements $M_{\mu\tau}$

The full expression of $M_{\mu\tau}$ element in the 3+1 scenario is given by

$$\begin{aligned} M_{\mu\tau} = & e^{i(2\delta_{14}-\delta_{24}+2\gamma)} c_{14}^2 c_{24} m_4 s_{24} s_{34} \quad (56) \\ & + e^{2i(\delta_{13}+\beta)} m_3 (c_{13} c_{24} s_{23} - e^{i(\delta_{14}-\delta_{24}-\delta_{13})} s_{13} s_{14} s_{24}) \{ -e^{i(\delta_{14}-\delta_{13})} c_{24} s_{13} s_{14} s_{34} \\ & + c_{13} (c_{23} c_{34} - e^{i\delta_{24}} s_{23} s_{24} s_{34}) \} + m_1 \{ -c_{23} c_{24} s_{12} \\ & + c_{12} (-e^{i\delta_{13}} c_{24} s_{13} s_{23} - e^{i(\delta_{14}-\delta_{24})} c_{13} s_{14} s_{24}) \} \\ & [-s_{12} (-c_{34} s_{23} - e^{i\delta_{24}} c_{23} s_{24} s_{34}) + c_{12} \{ -e^{i\delta_{14}} c_{13} c_{24} s_{14} s_{34} - e^{i\delta_{13}} s_{13} (c_{23} c_{34} - e^{i\delta_{24}} s_{23} s_{24} s_{34}) \} \} \\ & + e^{2i\alpha} m_2 \{ c_{12} c_{23} c_{24} \\ & + s_{12} (-e^{i\delta_{13}} c_{24} s_{13} s_{23} - e^{i(\delta_{14}-\delta_{24})} c_{13} s_{14} s_{24}) \} \\ & [c_{12} (-c_{34} s_{23} - e^{i\delta_{24}} c_{23} s_{24} s_{34}) \\ & + s_{12} \{ -e^{i\delta_{14}} c_{13} c_{24} s_{14} s_{34} \\ & - e^{i\delta_{13}} s_{13} (c_{23} c_{34} - e^{i\delta_{24}} s_{23} s_{24} s_{34}) \} \}. \end{aligned}$$

For NH, when m_1 is zero, using the approximations as defined in Eqs. (37, 18) and putting the Majorana phases equals

to zero and the Dirac phases equals to 180° , the above equation simplifies to

$$\begin{aligned} & |c_{23} c_{34} s_{23} (1 - c_{12}^2 \sqrt{R_{\nu}}) \quad (57) \\ & + \lambda \{ (c_{12} c_{34} s_{12} \sqrt{R_{\nu}} a_{13}) \cos 2\theta_{23} \\ & + a_{24} s_{34} (s_{23}^2 + c_{12}^2 c_{23}^2 \sqrt{R_{\nu}}) \\ & + s_{34} (\sqrt{R_{\nu}} a_{24} + c_{12} c_{23} s_{12} \sqrt{R_{\nu}} a_{14}) \} \\ & + \lambda^2 \{ s_{12} a_{13} s_{23} s_{34} \sqrt{R_{\nu}} (s_{12} a_{14} + 2c_{12} c_{23} a_{24}) \\ & + a_{14} s_{23} (c_{12} c_{34} s_{12}^2 s_{23} \sqrt{R_{\nu}} a_{13}^2) \} = 0. \end{aligned}$$

From the above equation we can see that the $R_{\nu 1}$ appears with both θ_{14} and θ_{24} . Thus cancellation of sterile term with the active neutrino terms will not be possible when both these parameters are very large. This is evident from the upper left panel of Fig. (7) from where we notice that when s_{34}^2 is small (high), s_{24}^2 is high (small). But note that when both the angles are very small, then the active part becomes larger than the sterile term and cancellation is again not possible. Here the bound of the effective mass M_{ee} is < 0.10 eV (top right panel of Fig. (7)). For IH when $m_3 = 0$, using the approximations of Eqs. (37, 18) the expression for $M_{\mu\tau}$ becomes,

$$\begin{aligned} M_{\mu\tau} \approx & \{ -c_{23} c_{34} s_{23} (c_{12}^2 e^{2i\alpha} + s_{12}^2) \quad (58) \\ & + \lambda [c_{12} s_{12} (1 - e^{2i\alpha}) (c_{34} \cos 2\theta_{23} e^{i\delta_{13}} a_{13} \\ & + c_{23} s_{34} e^{i\delta_{14}} a_{14}) \\ & + s_{34} \{ e^{i(2\gamma+2\delta_{14}-\delta_{24})} \sqrt{R_{\nu 1}} \\ & - c_{23}^2 e^{i\delta_{24}} (s_{12}^2 + c_{12}^2 e^{2i\alpha}) \} a_{24}] \\ & + \lambda^2 [c_{23} c_{34} s_{23} e^{2i\delta_{13}} (c_{12}^2 + e^{2i\alpha} s_{12}^2) a_{13}^2 \\ & + c_{12} s_{12} s_{23} (e^{2i\alpha} - 1) (c_{34} e^{i(\delta_{14}-\delta_{24})} a_{14} \\ & + 2s_{34} c_{23} e^{i(\delta_{13}+\delta_{24})} a_{13}) a_{24} \}]. \end{aligned}$$

Taking $\alpha = 0^\circ$ and either $\theta_{34} = 0^\circ$ or $\theta_{24} = 0^\circ$ the above equation simplifies to

$$M_{\mu\tau} = -c_{23} c_{34} s_{23} (1 + s_{13}^2 e^{2i\delta_{13}}) \quad (59)$$

Thus the texture $|M_{\mu\tau}| = 0$ will be disallowed in IH for very small values of θ_{24} and θ_{34} when $\alpha = 0^\circ$ but will be allowed when the $R_{\nu 1}$ term becomes of the same order as the term in Eq. (59). As when α approaches to $\pi/2$, the other terms start to contribute and thus one can have cancellations for small values of the above mentioned sterile mixing angles. This can be seen from the middle left panel of Fig. (7). Here we notice that for $\alpha = 0, \pi$ the allowed range of $s_{24}^2 s_{34}^2$ is (0.0002 - 0.001) and for $\alpha = \pi/2$, we obtain $s_{24}^2 s_{34}^2 < 0.0004$. In this case the effective mass has an upper bound of 0.013 eV.

The correlation plots for $|M_{\mu\tau}| = 0$ for QD neutrino mass spectrum are given in the lower panels of Fig (7). The expression for this texture is quite complicated and to understand the correlations between parameters we take the Majorana phases $\alpha = 90^\circ$ and $(\beta + \delta_{13}) = 0^\circ$ and vanishing Dirac phases δ_{14} and δ_{24} . These approximations gives the expression for zero texture at $M_{\mu\tau}$ as,

$$\begin{aligned} & | \sin 2\theta_{23} c_{12}^2 c_{34} m_0 + [-a_{24} s_{34} (m_0 (s_{23}^2 - c_{23}^2 \cos 2\theta_{12}) \\ & - m_4) + m_0 \sin 2\theta_{12} (a_{13} e^{i\delta_{13}} \cos 2\theta_{23} + a_{14} c_{23} s_{34})] \lambda \\ & + \mathcal{O}(\lambda^2) | = 0. \quad (60) \end{aligned}$$

³ In this texture, we find that α is allowed in its full range.

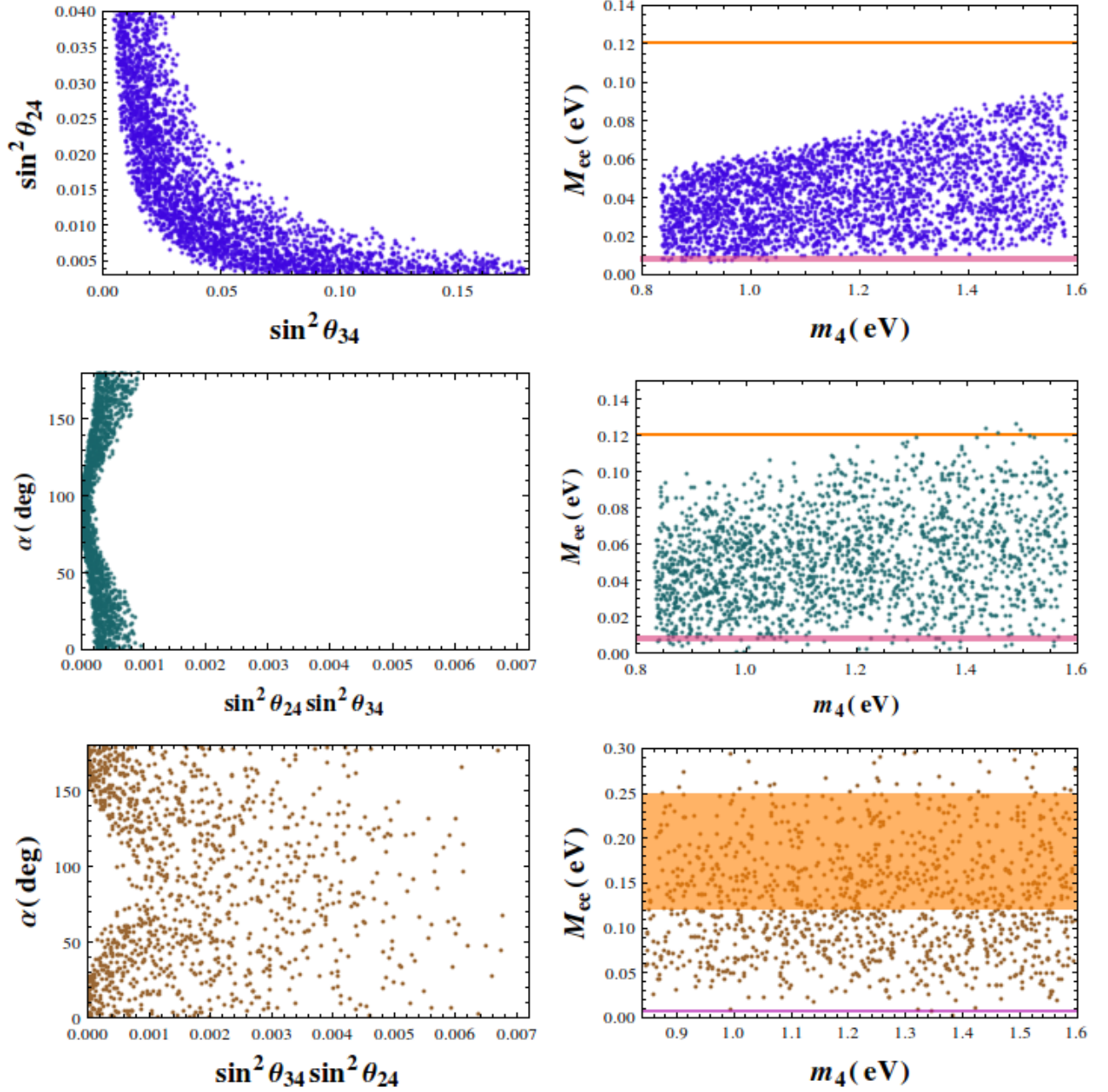


FIG. 7. Correlation plots for $|M_{\mu\tau}| = 0$ for NH (upper panel), IH (middle panel) and QD (lower panel) mass spectrum. Bounds on M_{ee} are described in the caption of Fig.(3).

The leading term ($\mathcal{O}(10^{-2})$) in this case is always greater than the subleading terms $\mathcal{O}(10^{-3})$ for very small values of $s_{24}s_{34}$. Therefore there is no allowed solution when $\alpha = 0^\circ$ and θ_{14} and θ_{24} are very small. On the other hand when we increase the value of $s_{24}s_{34}$ the subleading term with coefficient λ becomes sufficiently large and gets cancelled with the leading order term to give allowed points. These conclusions are quite clearly depicted in the lower left panel of Fig. (7).

E. The mass matrix element $M_{\tau s}$

The full expression for the element $M_{\tau s}$ is given by,

$$M_{\tau s} = c_{14}^2 c_{24}^2 c_{34} e^{2i(\delta_{14} + \gamma)} m_4 s_{34} + (m_1, m_2, m_3) \text{ terms.} \quad (61)$$

We note that the m_4 term appears with s_{34} . Thus it is clear that if θ_{34} is very high then the sterile term will be very large

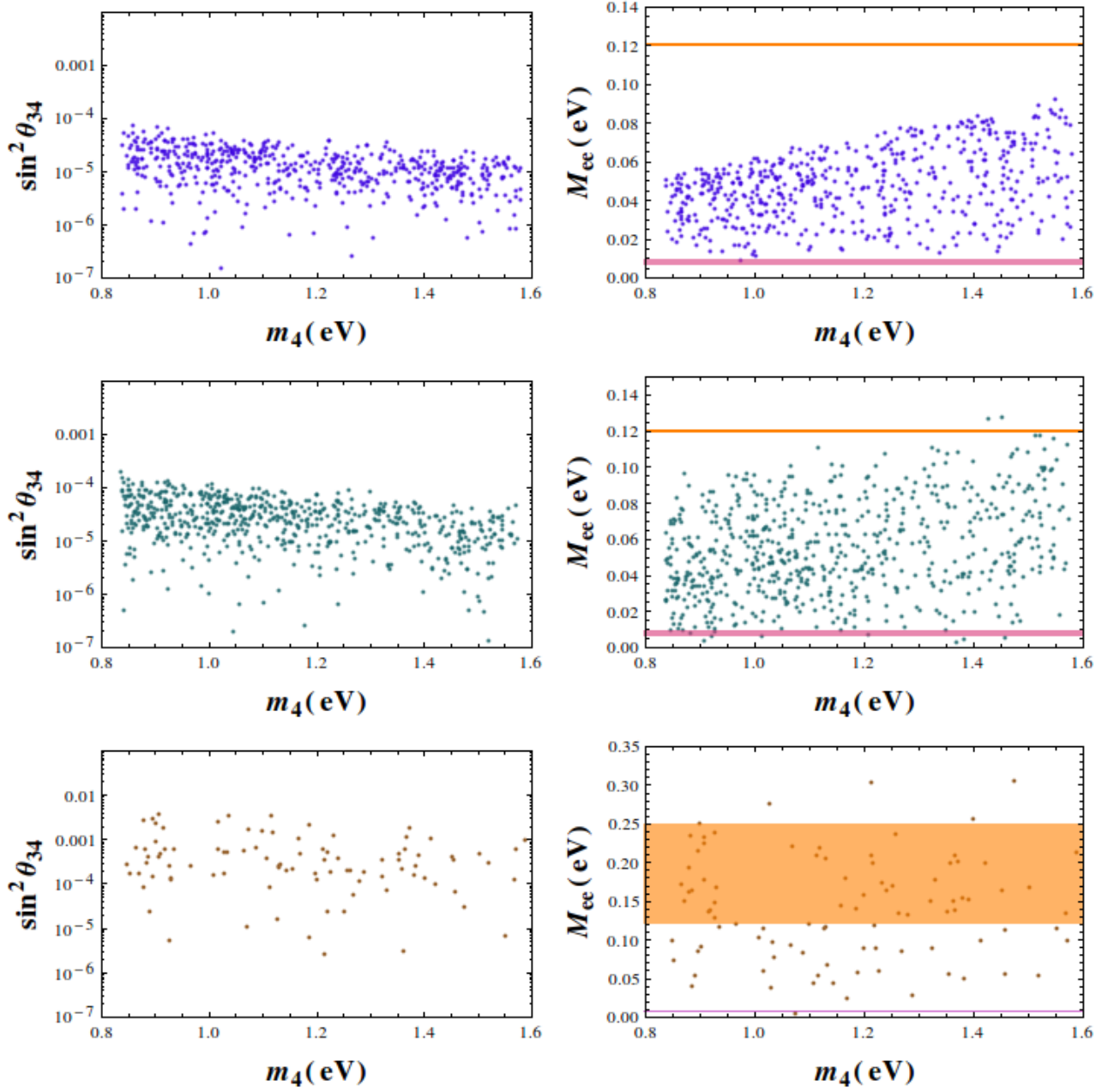


FIG. 8. Correlation plots for $|M_{\tau s}| = 0$ for NH (upper panel), IH (middle panel) and QD (lower panel) mass spectrum. Bounds on M_{ee} are described in the caption of Fig.(3).

and it is impossible to have cancellations with the active terms.

The texture $|M_{\tau s}| = 0$ in both NH and IH will be only possible for very small values of θ_{34} . This has been shown in the upper left and middle left panels of Fig. (8). In both the plots we note that as m_4 increases, the value of s_{34}^2 decreases. For both the hierarchies, the highest possible value of s_{34}^2 for which cancellation can occur is of the order of 10^{-4} . Here the effective mass M_{ee} is restricted within 0.10 eV (0.14 eV) in NH (IH) (upper (middle) right panels of Fig. (8)).

$|M_{\tau s}| = 0$ for QD is marginally allowed in the region $10^{-6} < s_{34}^2 < 0.01$ as reflected in the lower left panel of Fig (8). In this case, we note that the allowed values of θ_{34} are slightly higher as compared to the NH and IH case. This is because in the QD regime, the contributions from active terms are greater as compared to the completely hierarchical regime. Thus to have cancellation, the m_4 terms needs to be large, and that is why higher values of θ_{34} are preferred in this case.

F. The mass matrix elements M_{es} , $M_{\mu s}$ and M_{ss}

The zero textures at matrix elements M_{es} , $M_{\mu s}$ and M_{ss} are disallowed by the current data if we assume that the lowest mass vanishes. This can be understood by looking at the m_4 terms of these elements.

$$\begin{aligned} M_{es} &= c_{14}c_{24}c_{34}e^{2i(\delta_{14}+\gamma)}m_4s_{14} \\ &\quad + (m_1, m_2, m_3)\text{terms}, \\ M_{\mu s} &= c_{14}^2c_{24}c_{34}e^{2i(\delta_{14}+\gamma)}m_4s_{24} \\ &\quad + (m_1, m_2, m_3)\text{terms}, \\ M_{ss} &= c_{14}^2c_{24}^2c_{34}^2e^{2i(\delta_{14}+\gamma)}m_4 \\ &\quad + (m_1, m_2, m_3)\text{terms}. \end{aligned} \quad (62)$$

In the elements M_{es} and $M_{\mu s}$ we see that the m_4 term appears with s_{14} and s_{24} respectively. Thus these terms are in general large and can be cancelled with the active terms only for the higher values of the lowest masses (m_1 for NH and m_3 for IH). Because when the lowest mass vanishes, the active terms become smaller than the m_4 term and thus cancellation is not possible. For M_{ss} , we see that the m_4 term is not suppressed by the sterile mixing angles and thus it is of the order of ~ 1 eV. For this reason, it is never possible to have $|M_{ss}| = 0$ for NH, IH and QD mass spectrum.

For the QD scenario, the condition for texture zero for M_{es} is given by,

$$\begin{aligned} &|c_{12}s_{23}s_{34}s_{12}m_0(e^{2i\alpha} - 1) + (a_{14}c_{34}e^{i\delta_{14}}(m_0(c_{12}^2 + s_{12}^2e^{2i\alpha}) - m_4e^{2i\gamma}) - m_0c_{23}(a_{24}c_{12}c_{34}e^{i\delta_{24}}(e^{2i\alpha} - 1)s_{12} \\ &\quad + a_{13}e^{i\delta_{13}}(-(c_{12}^2 + s_{12}^2e^{2i\alpha}) + e^{2i\beta})s_{34})))\lambda + \mathcal{O}(\lambda^2)| = 0 \end{aligned} \quad (63)$$

By looking at the above expression we can conclude that even when active neutrinos are quasidegenerate, it is not possible to have $|M_{es}| = 0$. This is because the term $m_4 \sin \theta_{14}$ which appears with a coefficient λ , has far greater magnitude ($\sim 10^{-1}$) than the other two terms.

Regarding $|M_{\mu s}|$ we find that, this element can marginally vanish in the QD mass spectrum. Using the approximations for QD and Eq. (37) the zero texture condition of $M_{\mu s}$ translates to:

$$\begin{aligned} &|-c_{23}s_{23}s_{34}m_0(-c_{12}^2e^{2i\alpha} + e^{2i(\beta+\delta_{13})} - s_{12}^2) + e^{-i\delta_{24}}(-a_{24}c_{34}(c_{12}^2c_{23}^2e^{2i(\alpha+\delta_{24})}m_0 - e^{2i(\gamma+\delta_{14})}m_4 \\ &\quad + c_{23}^2s_{12}^2e^{2i\delta_{24}}m_0 + s_{23}^2e^{2i(\beta+\delta_{13}+\delta_{24})}s_{23}^2m_0) \\ &\quad c_{12}s_{12}e^{i\delta_{24}}(e^{2i\alpha} - 1)m_0(a_{14}c_{23}c_{34}e^{i\delta_{14}} \\ &\quad - a_{13}e^{i\delta_{13}}(c_{23}^2 - s_{23}^2)s_{34}))\lambda + \mathcal{O}(\lambda^2)| = 0 \end{aligned} \quad (64)$$

We have given the correlation plots for this texture in Fig. (9). Taking all the Majorana and the Dirac phases to be zero, we find that for the smaller values of θ_{24} , all the terms in the above expression are of the same order ($\mathcal{O}(10^{-1})$) and thus there are viable solutions. This can be seen from the left panel of Fig (9).

$M_{\alpha\beta=0}$	NH($m_1 = 0$)	IH($m_3 = 0$)	QD
M_{ee}	\times	\checkmark	\checkmark
$M_{e\mu}$	\checkmark	\checkmark	\checkmark
$M_{e\tau}$	\checkmark	\checkmark	\checkmark
$M_{\mu\tau}$	\checkmark	\checkmark	\checkmark
$M_{\mu\mu}$	\checkmark	\checkmark	\checkmark
$M_{\tau\tau}$	\checkmark	\checkmark	\checkmark
M_{es}	\times	\times	\times
$M_{\mu s}$	\times	\times	\checkmark
$M_{\tau s}$	\checkmark	\checkmark	\checkmark
M_{ss}	\times	\times	\times

TABLE II. Possible zero-textures that are allowed (disallowed) and these are marked with \checkmark (\times) for the three mass patterns when the parameters are varied in their allowed 3σ range.

V. CONCLUSIONS

We present the phenomenological analysis of one-zero texture of 4×4 low energy neutrino mass matrix (M_ν) in presence of an extra sterile neutrino in addition to the three active ones (3+1 scenario). To analyse the behaviour of active sterile mixing parameters we consider two different scenarios: (i) completely hierarchical mass spectrum of active neutrinos with vanishing lowest mass (i.e., NH and IH) (ii) completely quasidegenerate active neutrino masses where all the active neutrinos have almost equal mass (i.e., QD). This symmetric matrix M_ν has 10 independent entries and thus in general have 10 possible structures with one-zero texture. We extensively study the viability and correlation between different parameters of all these textures for both the cases using the neutrino oscillation data for active neutrinos [1–3] and the SBL data for active sterile mixing [34, 36]. For completely hierarchical mass spectrum only 7 texture zero structures are consistent with the current data and 8 are consistent for quasidegenerate mass spectrum. In Table (II), we have summarize the allowed and disallowed one-zero textures in neutrino mass matrix for both the mass spectrum under consideration. To understand our numerical results, we expand the matrix elements in terms of the small parameters by keeping the terms upto second order. We observe that the predictions of one-zero texture mass matrices change significantly when the cases corresponding to vanishing lowest active neutrino mass and quasidegenerate mass spectrum are compared. The texture $|M_{ee}| = 0$ is allowed only for IH and QD. The Majorana phase γ is highly constrained around $+90^\circ$ for both IH and QD, on the other hand, the other phase α is constrained only for QD masses. In 3-neutrino scenario, the element $M_{e\mu}$ and $M_{e\tau}$ are related by simple $\mu - \tau$ permutation symmetry but in 3+1 scenario, the relations are very complex as compared to the three generation case. Here the behaviour of θ_{24} in $M_{e\mu}$ is quite similar with the behaviour of θ_{34} in $M_{e\tau}$. We find that the texture $|M_{e\mu}| = 0$ mainly constrains the active sterile mixing an-

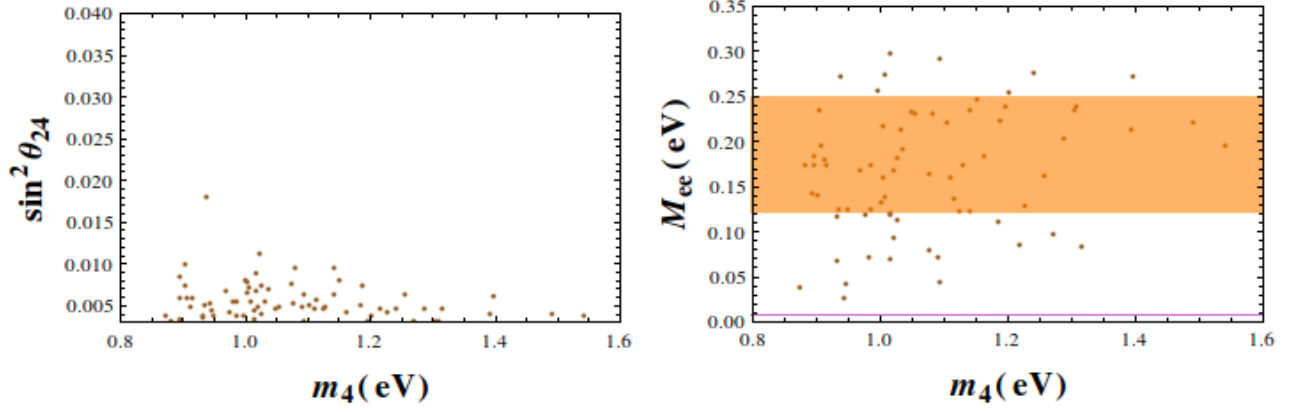


FIG. 9. Correlation plots for $|M_{\mu s}| = 0$ for QD mass spectrum. Band represents the allowed range of M_{ee} are described in the caption of Fig.(3).

gles θ_{14} , θ_{24} for NH and IH while for QD mass spectrum, the Majorana phase α is largely constrained for smaller values of θ_{24} . For vanishing $M_{e\tau}$ very small values of active sterile mixing angle θ_{34} is allowed for NH and IH. For QD spectrum Majorana phase α is constrained for small values of θ_{34} . The textures $|M_{\mu\mu}| = 0$ and $|M_{\tau\tau}| = 0$ are again related by $\mu - \tau$ symmetry and thus the characteristics of θ_{24} in $M_{\mu\mu}$ and θ_{34} in $M_{\tau\tau}$ are same. For $|M_{\mu\mu}| = 0$ and NH we find that very low and high values of s_{24}^2 are disallowed whereas for $|M_{\tau\tau}| = 0$ very low and high values of s_{34}^2 are disallowed. For IH we observe that for lower values of s_{24}^2 (s_{34}^2) most of the values of the Majorana phase α is disallowed in case of texture $M_{\mu\mu}$ ($M_{\tau\tau}$). For QD, however complete range of this angle is allowed for both these textures. For $|M_{\mu\tau}| = 0$ to be phenomenologically viable, the mixing angle θ_{24} and θ_{34} can not be very large or small simultaneously for NH. For IH the behaviour of α vs $s_{24}^2 s_{34}^2$ is same as that of α vs s_{24}^2 (α vs s_{34}^2) in $M_{\mu\mu}$ ($M_{\tau\tau}$). For QD, $\alpha = +90^\circ$ is not allowed for very small values of θ_{24} and θ_{34} . For $M_{\tau s}$ to vanish, the parameter s_{34}^2 should be as low as 10^{-4} irrespective of the hierarchy (NH or IH). However, for QD slightly higher values of θ_{34} are preferred. The remaining three textures M_{es} , $M_{\mu s}$ and M_{ss} are phenomenologically disallowed when we consider completely hierarchical mass spectrum with a vanishing neutrino mass. The sterile contribution in the first two cases $\propto m_4 s_{14}$ and $m_4 s_{24}$ respectively. These terms are in general large and there is no cancellation possible for these terms when the lowest mass is vanishing. However, for QD $|M_{\mu s}| = 0$ is marginally allowed for very small values of θ_{24} . The texture, M_{ss} is of the order of $\mathcal{O}(1)$ eV and hence it is not possible to get contributions of this order from the active sector for NH (IH) and QD mass spectrum.

The results discussed in the above paragraph are obtained by varying the neutrino oscillation parameters in their allowed 3σ range. However, we know that there are several current and future experiments which are expected to put a more stringent constrain on the active-sterile mixing parameters [49–51]. To

check what happens to allowed textures if the mixing angles are constrained furthermore, we re-evaluate the viability of the textures by varying the oscillation parameters in their allowed 1σ and 2σ allowed range as given in Table I. We find that the texture $M_{\mu s}$ is disallowed for QD when the parameters are varied within their 1σ range and the same is marginally allowed when the parameters are varied in their 2σ range. Apart from this, the other conclusions remain unaltered.

For all allowed textures in completely hierarchical and quasidegenerate scenarios we obtain the bounds on the effective mass M_{ee} that will be constrained by the forthcoming neutrinoless double beta decay experiments. For NH, the values of M_{ee} are well below the present bound and for IH it is within the present upper bound. In all the allowed textures we see that the upper bound on M_{ee} for NH is slightly smaller as compared to IH. For QD mass spectrum the some of the allowed region of the parameter space can be discarded from the bounds available on M_{ee} . The similar behaviours of M_{ee} for NH, IH and QD for all the allowed textures can be qualitatively understood from the following arguments. For NH, the m_2 and m_3 terms are proportional to the Δm_{21}^2 and Δm_{31}^2 respectively. On the other hand for IH and QD, all the active masses m_i ($i = 1, 2$ for IH and $i = 1, 2, 3$ for QD) are proportional to Δm_{31}^2 and $0.1 - 0.3$ eV² respectively. Thus we see that for NH, due to smaller values of the m_2 term, the prediction for M_{ee} is lower. Whereas for IH and QD, M_{ee} gets contribution from the large values of m_i and thus the prediction of M_{ee} is high for IH and even higher for QD as compared to NH.

If future experiments confirm the existence of a light sterile neutrino then the next challenge will be to build models for such scenarios. The texture analysis performed in this paper can be a useful guide for constructing models for light sterile neutrinos.

VI. ACKNOWLEDGEMENTS

The authors would like to thank Srubabati Goswami for her careful reading of the manuscript and helpful suggestions.

They would also like to thank Ujjal Dey for useful discussions. MG would like to thank Abhay Swain for help in Jaxo-draw. The work of SG is supported by the Australian Research Council through the ARC Center of Excellence in Particle Physics (CoEPP Adelaide) at the Terascale (CE110001004).

-
- [1] M. C. Gonzalez-Garcia, M. Maltoni, and T. Schwetz (2015), 1512.06856.
 - [2] D. V. Forero, M. Tortola, and J. W. F. Valle, Phys. Rev. **D90**, 093006 (2014), 1405.7540.
 - [3] F. Capozzi, G. L. Fogli, E. Lisi, A. Marrone, D. Montanino, and A. Palazzo, Phys. Rev. **D89**, 093018 (2014), 1312.2878.
 - [4] C. Athanassopoulos et al. (LSND), Phys.Rev.Lett. **77**, 3082 (1996), nucl-ex/9605003.
 - [5] C. Athanassopoulos et al. (LSND), Phys.Rev.Lett. **81**, 1774 (1998), nucl-ex/9709006.
 - [6] A. Aguilar-Arevalo et al. (LSND), Phys.Rev. **D64**, 112007 (2001), hep-ex/0104049.
 - [7] A. A. Aguilar-Arevalo et al. (MiniBooNE), Phys. Rev. Lett. **110**, 161801 (2013), 1207.4809.
 - [8] G. Mention, M. Fechner, T. Lasserre, T. Mueller, D. Lhuillier, et al., Phys.Rev. **D83**, 073006 (2011), 1101.2755.
 - [9] C. Giunti and M. Laveder, Phys.Rev. **C83**, 065504 (2011), 1006.3244.
 - [10] P. A. R. Ade et al. (Planck) (2015), 1502.01589.
 - [11] P. H. Frampton, S. L. Glashow, and D. Marfatia, Phys.Lett. **B536**, 79 (2002), hep-ph/0201008.
 - [12] S. Dev, S. Kumar, S. Verma, and S. Gupta, Phys.Rev. **D76**, 013002 (2007), hep-ph/0612102.
 - [13] Z.-z. Xing, Phys.Lett. **B530**, 159 (2002), hep-ph/0201151.
 - [14] Z.-z. Xing, Phys.Lett. **B539**, 85 (2002), hep-ph/0205032.
 - [15] B. R. Desai, D. Roy, and A. R. Vaucher, Mod.Phys.Lett. **A18**, 1355 (2003), hep-ph/0209035.
 - [16] S. Dev, S. Kumar, S. Verma, and S. Gupta, Phys.Lett. **B656**, 79 (2007), 0708.3321.
 - [17] S. Dev, S. Kumar, S. Verma, and S. Gupta, Nucl.Phys. **B784**, 103 (2007), hep-ph/0611313.
 - [18] S. Kumar, Phys.Rev. **D84**, 077301 (2011), 1108.2137.
 - [19] H. Fritzsch, Z.-z. Xing, and S. Zhou, JHEP **1109**, 083 (2011), 1108.4534.
 - [20] D. Meloni and G. Blankenburg, Nucl.Phys. **B867**, 749 (2013), 1204.2706.
 - [21] P. Ludl, S. Morisi, and E. Peinado, Nucl.Phys. **B857**, 411 (2012), 1109.3393.
 - [22] W. Grimus and P. Ludl, J.Phys. **G40**, 055003 (2013), 1208.4515.
 - [23] W. Grimus, A. S. Joshipura, L. Lavoura, and M. Tanimoto, Eur. Phys. J. **C36**, 227 (2004), hep-ph/0405016.
 - [24] C. I. Low, Phys. Rev. **D71**, 073007 (2005), hep-ph/0501251.
 - [25] S. Dev, S. Gupta, and R. R. Gautam, Phys. Lett. **B701**, 605 (2011), 1106.3451.
 - [26] M. Ghosh, S. Goswami, and S. Gupta, JHEP **04**, 103 (2013), 1211.0118.
 - [27] M. Ghosh, S. Goswami, S. Gupta, and C. S. Kim, Phys. Rev. **D88**, 033009 (2013), 1305.0180.
 - [28] Y. Zhang, Phys.Rev. **D87**, 053020 (2013), 1301.7302.
 - [29] E. I. Lashin and N. Chamoun, Phys. Rev. **D85**, 113011 (2012), 1108.4010.
 - [30] J. Barry, W. Rodejohann, and H. Zhang, JHEP **1107**, 091 (2011), 1105.3911.
 - [31] H. Zhang, Phys. Lett. **B714**, 262 (2012), 1110.6838.
 - [32] P. S. Bhupal Dev and A. Pilaftsis, Phys. Rev. **D87**, 053007 (2013), 1212.3808.
 - [33] C. Giunti and M. Laveder, Phys. Rev. **D84**, 073008 (2011), 1107.1452.
 - [34] T. Schwetz (2011), talk given at Proceedings of Sterile Neutrino Crossroads, 2011, Virginia Tech, USA.
 - [35] S. Goswami and W. Rodejohann, Phys.Rev. **D73**, 113003 (2006), hep-ph/0512234.
 - [36] J. Kopp, P. A. N. Machado, M. Maltoni, and T. Schwetz, JHEP **05**, 050 (2013), 1303.3011.
 - [37] P. Gorla (CUORE), J.Phys.Conf.Ser. **375**, 042013 (2012).
 - [38] J. Wilkerson, E. Aguayo, F. Avignone, H. Back, A. Barabash, et al., J.Phys.Conf.Ser. **375**, 042010 (2012).
 - [39] A. Barabash (SuperNEMO), J.Phys.Conf.Ser. **375**, 042012 (2012).
 - [40] A. Gando et al. (KamLAND-Zen), Phys.Rev.Lett. **110**, 062502 (2013), 1211.3863.
 - [41] M. Auger et al. (EXO), Phys.Rev.Lett. **109**, 032505 (2012), 1205.5608.
 - [42] S. Dell’Oro, S. Marcocci, and F. Vissani, Phys.Rev. (????).
 - [43] A. Merle and W. Rodejohann, Phys. Rev. **D73**, 073012 (2006), hep-ph/0603111.
 - [44] R. R. Gautam, M. Singh, and M. Gupta, Phys. Rev. **D92**, 013006 (2015), 1506.04868.
 - [45] C. S. Lam, Phys. Rev. **D71**, 093001 (2005), hep-ph/0503159.
 - [46] W. Grimus and L. Lavoura, Acta Phys. Polon. **B32**, 3719 (2001), [Acta Astron.32,3719(2001)], hep-ph/0110041.
 - [47] R. N. Mohapatra and W. Rodejohann, Phys. Rev. **D72**, 053001 (2005), hep-ph/0507312.
 - [48] S. Gupta, A. S. Joshipura, and K. M. Patel, JHEP **09**, 035 (2013), 1301.7130.
 - [49] F. P. An et al. (Daya Bay) (2016), 1607.01174.
 - [50] P. Adamson et al. (MINOS) (2016), 1607.01176.
 - [51] P. Adamson et al. (MINOS, Daya Bay), Submitted to: Phys. Rev. Lett. (2016), 1607.01177.